Available online at www.sciencedirect.com
ScienceDirect
Journal of Sound and Vibration 309 (2008) 426–464
JOURNAL OF SOUND AND VIBRATION
www.elsevier.com/locate/jsvi

The behavior of higher order mode shape derivatives in damaged, beam-like structures

Timothy M. Whalen*

School of Civil Engineering, Purdue University, 550 Stadium Mall Drive, West Lafayette, IN 47907-2051, USA

Received 26 September 2006; received in revised form 12 July 2007; accepted 18 July 2007
Available online 3 October 2007

Abstract

This work considers the effect that damage has upon the higher order derivatives of mode shapes of structures having primarily beam-like vibration. Via numerical investigations, the sensitivity of various damage related parameters in inducing changes in these higher order modal derivatives is determined, leading to a more complete understanding of what factors make the most contribution to significant changes in these derivatives. It is concluded that higher order mode shape derivatives (e.g., modal curvature, third derivative, and fourth derivative) are better indicators of damage than the mode shapes. Three distinct types of response for the damage-induced higher order derivative discontinuities are identified as three key parameters (the mass loss, stiffness loss, and damage radius scale) vary. From this, formal approximations are obtained for the expected forms of the higher order derivative discontinuities based upon the underlying behavior predicted by a simple relation among these three parameters. These approximations are checked with numerical simulations, and an excellent level of agreement is observed under appropriate conditions. Finally, the potential of these higher order derivative changes for indicating the presence and location of damage in a global setting is examined.

1. Introduction

A great deal of interest has developed over the past few decades in developing methods to detect, locate, and quantify damage in civil infrastructure (i.e., structural health monitoring) by determining changes in a structure's vibration characteristics. Such methods are popular due to the relative ease in which vibration tests can be performed and the direct relationships that exist between structural properties and vibration-response properties. Excellent reviews of the literature related to structural health monitoring and damage identification methods based upon vibration changes are given in Refs. [1,2].

One of two conceptual strategies forms the basis for most damage identification methods presented in the literature. One strategy centers on "model-based" approaches [3], in which experimentally obtained vibration data are used to update a model of the current state of the structure, from which changes relative to a previous state can be identified. The model may be explicitly defined (e.g., a finite element model of the structure) or implicitly defined (e.g., a neural network trained to relate structural properties and vibration response

*Tel.: +1 765 494 2225; fax: +1 765 494 0395.
E-mail address: whalen@purdue.edu

0022-460X/$ - see front matter
doi:10.1016/j.jsv.2007.07.054

quantities). Several problems have been identified with such strategies [4], including an inability to guarantee accurate modeling of the structure to be monitored, difficulty in accounting for errors in the measurements, and a lack of uniqueness in the relationship between updated structural properties and resulting vibration responses. In this work, such methods are not considered.

The second conceptual strategy may be termed as "response-based" approaches [3]. In these methods, various response signals are analyzed to identify features that may be associated with damage. While often limited to detecting or locating damage, such approaches have been deemed very effective [2] since they avoid modeling issues and can accommodate techniques for dealing with measurement error. They also have the potential to be implemented in automated procedures, thus leading to real-time health monitoring. Given these advantages over model-based methods, it is useful to consider applications of response-based methods to damage identification in civil infrastructure systems.

A fundamental issue in any response-based approach to damage identification is the selection of an appropriate signal feature to monitor [5]. A wide variety of signal features have been proposed for use in damage identification, including resonant frequencies [6], mode shapes [7], mode shape slopes [8], mode shape curvatures [9], strain energies [10], frequency response functions [11], nonlinear response features [12], wave propagation parameters [13], autocorrelation functions [14], wavelet coefficients [15], modal damping [16], intrinsic mode functions [17], and auto-regressive coefficients of acceleration time histories [18]. (This list is not intended to be comprehensive in either the features or the researchers shown. Refer to the previously cited literature reviews for further information.) Two important factors influencing the viability of any given feature in the damage identification process are (a) its sensitivity to small, localized damage, which influences the ability to detect damage at an early stage, thus increasing the chances for successful repair, and (b) the ability to distinguish signal features due to damage from features arising from other sources such as the feature extraction process or variability in the testing environment [1]. An ideal feature for use in damage identification should be sensitive to small changes induced by damage as well as robust in the presence of measurement and calculation errors.

Among researchers who have utilized features associated with modal vibration properties of a structure, it is often concluded [9,19] that changes in mode shapes, and particularly mode shape curvatures, are sensitive to the presence and location of damage and thus make good candidates for a damage identification feature. These sensitivity properties, however, have not been studied systematically and are often validated only by anecdotal results for specific structures [1]. In addition, it has been observed [20] that relatively large levels of damage are used by many researchers when studying the sensitivity of mode shapes to damage, making it unclear whether the proposed feature would be capable of identifying incipient damage.

In this work, we undertake an examination of the behavior of higher order derivatives (e.g., second, third, and fourth derivatives) of modes shapes in the presence of damage. We restrict our analysis to beam-like structures whose dominant vibration modes are transverse. While this limits the applicability of the results, they are still relevant to a significant class of structures, including bridges. We are interested in determining the sensitivity of these higher order modal derivatives to various damage-related parameters, with an eye towards identifying parameters that have the most impact upon the magnitude of the damage-induced changes in the modal derivatives. Based on this, we wish to determine the ability of the higher order modal derivatives to have strong changes due to damage. We perform numerical studies of the vibration equations and use these results to motivate analytical approximations for the changes induced by damage. Finally, we discuss the utility of mode shape derivatives as damage identification features and make recommendations for features to consider.

2. Theoretical considerations

2.1. Modeling of transverse vibrations for damaged structures

In this work, we assume that the transverse vibrations of the structure to be monitored can be described by Euler–Bernoulli beam theory. This implies that shear deformations of the structure in question are negligible, as is the effect of rotary inertia. We ignore the possibility of coupled torsional-flexural bending motions, which may actually be present in long-span bridges and other highly flexible structures. We allow for axial variations

in both the flexural rigidity EI as well as the mass density per unit length ρA. Under these assumptions, the governing equation for free vibration of the structure is

$$\frac{\partial^2}{\partial x^2}\left[EI(x)\frac{\partial^2 y}{\partial x^2}\right] + \rho A(x)\frac{\partial^2 y}{\partial t^2} = 0, \tag{1}$$

where $y(x,t)$ is the total transverse displacement. Standard separation of variables arguments [21] lead to the corresponding equation governing the mode shapes:

$$\frac{\mathrm{d}^2}{\mathrm{d}x^2}\left[EI(x)\frac{\mathrm{d}^2 Y_n(x)}{\mathrm{d}x^2}\right] - \omega_n^2 \rho A(x) Y_n(x) = 0, \tag{2}$$

where $Y_n(x)$ and ω_n are the nth mode shape and natural frequency of vibration. (Boundary conditions must be included in order to determine the natural frequencies.) For simplicity, we shall assume that the mode shapes are nondimensional and are scaled to have a maximum value of one.

We next consider models for the effect of damage upon the flexural rigidity and the mass density. There are many approaches used in the literature to model the effect of damage on flexural rigidity. For example, several authors (e.g., Refs. [22,23]) have used discontinuous distribution functions to model stiffness changes. Such models take the general form

$$EI(x) = EI_o\{1 - \theta D(x - x_d)\}, \tag{3}$$

where EI_o is a nominal flexural rigidity of the beam, θ relates to the "size" of the discontinuity, and $D(x-x_d)$ is a discontinuous distribution such as the Heaviside step function $H(x-x_d)$ or Dirac delta function $\delta(x-x_d)$ associated with a change in rigidity at $x = x_d$. Such models are consistent with the assumption of a "jump" or "step" discontinuity in the flexural stiffness. A variation on such a model is the use of a pair of "jumps"—one that decreases the stiffness while the other increases it. This version is implicitly assumed in many finite element-based models where damage is simulated by modifying element stiffnesses.

Another class of flexural rigidity models is associated with so-called cracked beam theory, in which modifications of the stress and strain fields due to the presence of one or more open cracks in a beam lead to changes in the effective stiffness in a neighborhood of the crack(s) [24–27]. An illustration of applying cracked beam theory to an Euler–Bernouli beam with a rectangular cross section and a pair of symmetric open cracks is provided in Ref. [24]; the resulting flexural rigidity function is

$$EI(x) = EI_o\left\{1 + \frac{m-1}{\exp\left[\dfrac{2\alpha}{d}|x - x_d|\right]}\right\}^{-1}. \tag{4}$$

In this model, m is a constant related to the stress distribution on the cracked section, $2d$ is the depth of the beam, and α describes the rate of stress decay away from the crack tip. Variations of such models have been utilized [28,29], among others.

A common feature of most flexural rigidity models is the presence of a characteristic "radius" l_d associated with the axial region in which the flexural rigidity is expected to differ from its undamaged value. For instance, setting $m = 1.2$ in the illustrative function in Eq. (4), we note that $EI_o - EI(x) < 0.0001EI_o$ for $|x - x_d| > 3.8d/\alpha \equiv l_d$; it is reasonable to conclude that the effect of the crack on the stiffness is confined to the region $x_d - l_d \leqslant x \leqslant x_d + l_d$. As mentioned previously, many finite element models also have such a radius, arising from the finite-sized zone of reduced stiffness. The presence of l_d (either explicitly or implicitly) reflects the intuitive assumption that the effect of damage is spatially bounded in some sense; this assumption plays a vital role in the subsequent analysis.

Based upon the above observations, we model the flexural rigidity of the damaged beam as follows:

$$EI(x) = EI_o\{1 - \kappa\Delta(\eta(x))\}, \tag{5}$$

where $\eta(x) = (x - x_d)/l_d$ is a dimensionless "damage zone" coordinate whose origin is $x = x_d$ (the damage center), $\Delta(\eta)$ is a nondimensional, $\mathscr{C}^2$-continuous stiffness modification function expressing the flexural rigidity changes due to damage, and κ is the maximum percentage change in $EI(x)$ from its undamaged value EI_o.

Note that the continuity requirement in principle rules out models of the form shown in Eq. (3). We can, however, overcome this obstacle by considering appropriately continuous functions whose limiting behavior is discontinuous. It is assumed that $0 \leqslant \Delta(\eta) \leqslant 1$ for all values of η and that Δ and its derivatives with respect to its argument are zero for $|\eta| > 1$ (i.e., outside of the "damage zone"). It is also assumed that $\Delta(\eta = 0) = 1$. (This last assumption is consistent with the assumption of a symmetric damage zone; while convenient, we note that such symmetry is not required.) As for $\rho A(x)$, it was noted in Ref. [1] that most damage identification methods do not assume noticeable mass changes due to damage. One exception is Chondros [26], who related changes in linear momentum to a "displacement disturbance function", resulting in a functional form for $\rho A(x)$ similar to that of $EI(x)$. Thus, we assume that $\rho A(x)$ has features similar to those of $EI(x)$; that is

$$\rho A(x) = \rho A_o\{1 - \mu\Gamma(\eta(x))\}, \tag{6}$$

with the mass modification function $\Gamma(\eta)$ having properties similar to those of $\Delta(\eta)$ and μ representing the maximum percentage change in density from the undamaged value ρA_o.

2.2. Modal equation of motion in the presence of damage

Before determining the effect of damage as modeled by Eqs. (5) and (6) on the modal vibration equation, we consider solutions to the undamaged version of the problem. Setting $\kappa = \mu = 0$ and defining the parameter $\beta_{o,n}^4 = (\omega_{o,n}^2 \rho A_o)/EI_o$, where $\omega_{o,n}^2$ is the natural frequency of the undamaged nth mode, leads to undamaged mode shapes of the form

$$Y_{o,n}(x) = C_{1,n}\sin(\beta_{o,n}x) + C_{2,n}\cos(\beta_{o,n}x) + C_{3,n}\sinh(\beta_{o,n}x) + C_{4,n}\cosh(\beta_{o,n}x), \tag{7}$$

where the unknown coefficients $C_{i,n}$ are determined from the boundary conditions and the normalization condition $\max Y_{o,n}(x) = 1$. We note that, in general, the undamaged mode shapes have the property that their fourth derivative with respect to the axial coordinate is simply a scalar multiple of the mode shape itself, with $\beta_{o,n}^4$ being the scaling factor. We identify $L_{o,n} = \pi/2\beta_{o,n}$, which is one quarter-wavelength for the nth mode, as a characteristic axial length scale over which the displacements vary significantly. The details of these displacements depend upon the exact boundary conditions, but for our purposes it is enough to note that the displacement magnitude must reach a peak over a distance of $2L_{o,n}$, giving $L_{o,n}$ a radius-like property for displacements similar to that of l_d for damage. Comparisons between $L_{o,n}$ and l_d turn out to play an important role in determining the size of the perturbations to the mode shape derivatives caused by damage.

We next introduce a rescaling of Eq. (2) that accounts for the characteristic length scale of the given undamaged mode $Y_{o,n}(x)$:

$$\xi = x/L_{o,n}, \quad \xi_d = x_d/L_{o,n}, \quad \Lambda_k = L/L_{o,n}, \quad \lambda_d = l_d/L_{o,n}, \quad \Psi_n(\xi) = Y_n(\xi L_{o,n}), \quad \Psi_{o,n}(\xi) = Y_{o,n}(\xi L_{o,n}). \tag{8}$$

Performing these changes, as well as introducing the damage models from Eqs. (5) and (6), leads to the following:

$$\frac{1}{L_{o,n}^2}\frac{\mathrm{d}^2}{\mathrm{d}\xi^2}\left[EI_o\{1 - \kappa\Delta(\eta(\xi))\} \times \frac{1}{L_{o,n}^2}\frac{\mathrm{d}^2\Psi_k(\xi)}{\mathrm{d}\xi^2}\right] - \omega_n^2\rho A_o\{1 - \mu\Gamma(\eta(\xi))\}\Psi_n(\xi) = 0. \tag{9}$$

(Note that $\eta(\xi) = (\xi - \xi_d)/\lambda_d = (x - x_d)/l_d$; the rescaling leaves this variable invariant.) Using the definitions of $\beta_{o,n}$ and $L_{o,n}$, this equation can be simplified to

$$\frac{\mathrm{d}^2}{\mathrm{d}\xi^2}\left[\{1 - \kappa\Delta(\eta(\xi))\}\frac{\mathrm{d}^2\Psi_n(\xi)}{\mathrm{d}\xi^2}\right] - \left(\frac{\pi}{2}\right)^4\Omega_n^2\{1 - \mu\Gamma(\eta(\xi))\}\Psi_n(\xi) = 0. \tag{10}$$

The constant Ω_n in Eq. (10) is defined by $\Omega_n^2 = \omega_n^2/\omega_{o,n}^2$; it can be considered to represent the effect of natural frequency modification due to damage. This is our assumed general equation for the mode shapes of the damaged structure.

3. Numerical studies

We now study the behavior of the general mode shape equation in the presence of damage. Our purpose is to clarify the properties of the mode shapes and their derivatives, establish their sensitivity to various damage situations, and provide insight into their use in damage identification algorithms. Our approach is to obtain numerical solutions to Eq. (10), from which higher order derivatives and other pertinent quantities can be computed. All solutions were calculated using the *bvp4c* function in Matlab® with a relative error tolerance of 5×10^{-7} and an absolute error tolerance of 5×10^{-11}. This function enforces $\mathscr{C}^1$-continuity of the solution; such continuity is reasonable for this study since the beam is not expected to break or to form discrete hinges. The *bvp4c* procedure requires specification of an initial grid and an approximate solution of the governing equation on this grid. In this work, the size of the initial grid was set at 220 points, with finer grid resolution in the damage zone. The solution to the undamaged mode shape equation was taken as the initial approximate solution.

3.1. Simply supported beam problem

3.1.1. General information

The first problem to be considered is a uniform beam of length $L=1200$ units simply supported at each end; Fig. 1 shows the relevant details. (Note that the choice of units is irrelevant to the analysis, as long as the system is assumed to have beam-like behavior.) We assume that the damage zone is centered at $x=500$ units, while the damage zone radius l_d will be given various values to explore the effect of spatial concentration of damage. In the absence of damage, the following solutions are obtained for the mode shapes of the full equation and corresponding nondimensional equation:

$$Y_{o,n}(x)=\sin(\beta_{o,n}x),\quad \beta_{o,n}=\frac{n\pi}{L}\Leftrightarrow \Psi_{o,n}(\xi)=\sin\left(\frac{\pi\xi}{2}\right). \tag{11}$$

The nondimensional beam length corresponding to each mode is thus $\Lambda_n=2n$, and $\xi_d=5n/6$ for Mode n. We now wish to compare these solutions to solutions of Eq. (10) for various damage scenarios.

We utilize a very simple model of damage, in which it is assumed that a rectangular cross-sectioned beam (depth $=d_o$, width $=w_o$) loses depth due to damage in a symmetric fashion across the full width from both the top and bottom. This model is based on the same physical situation as the model used by Christides and Barr [24] and subsequent researchers, but it employs a much simpler approach to estimate the loss of mass and stiffness. (No claim is made here regarding the accuracy of this model; it is simply a convenient choice to illustrate behaviors.) We write the following function for the depth of the beam in the damage zone:

$$d(x)=d_o\{1-\delta\Xi(\eta(x))\}, \tag{12}$$

where $\Xi(\eta(x))$ describes the variation of depth loss with position and δ is the maximum percentage of total loss of depth. We make the simplifying assumption that $\Xi(\eta(x_d)=0)=1$. Under this model, loss of area (and hence loss of mass) is directly proportional to loss of beam depth, and the loss of moment of inertia (and thus stiffness) is related to the cube of $d(x)$. This allows us to make the following identifications:

$$\kappa\Lambda(\eta)=(3\delta-3\delta^2+\delta^3)\frac{3\delta\Xi(\eta)-3\delta^2\Xi(\eta)^2+\delta^3\Xi(\eta)^3}{3\delta-3\delta^2+\delta^3},\quad \mu\Gamma(\eta)=\delta\Xi(\eta). \tag{13}$$

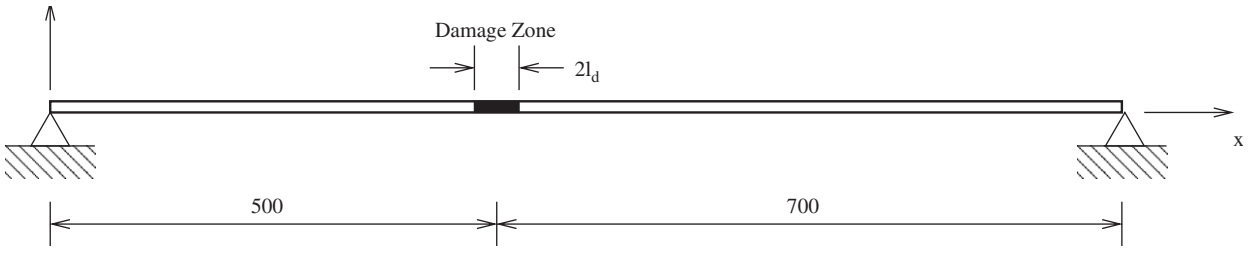

Fig. 1. The simply supported beam problem.

We assume that the loss of depth function is as follows:

$$\Xi(\eta) = \cos^3\left(\frac{\pi}{2}|\eta|^k\right), \quad |\eta| \leqslant 1. \tag{14}$$

This is a variation of the stiffness modification model used in Ref. [28], where the modification of the exponent on the cosine function is made in order to guarantee that $\Delta(\eta)$ and $\Gamma(\eta)$ are $\mathscr{C}^2$-continuous, even at the edges of the damage zone. This will ensure that there are no "spikes" or "jumps" in the coefficients of Eq. (10) that might generate discontinuities in the mode shape or its derivatives. In the following two subsections, the exponent of $|\eta|$ is fixed to $k = 1$.

3.1.2. Effect of damage level

Our first investigation considered the effect of damage magnitude on the behaviors of the mode shapes and their derivatives. We assumed a damage zone radius of $l_d = 12$ units, and we examined three levels of damage as expressed by the loss of depth parameter δ: "small" damage ($\delta = 0.003$), "moderate" damage ($\delta = 0.03$), and "large" damage ($\delta = 0.3$). The corresponding mass loss and stiffness loss parameters were thus $\mu = 0.003$ and $\kappa \approx 0.008973$ for small damage, $\mu = 0.03$ and $\kappa \approx 0.08733$ for moderate damage, and $\mu = 0.3$ and $\kappa = 0.657$ for large damage. We analyzed the first two modes of the beam; these are associated with characteristic modal lengths of $L_1 = 600$ units and $L_2 = 300$ units respectively, producing values of $\xi_d = 0.8333$ and $\lambda_d = 0.02$ for Mode 1 and $\xi_d = 1.6667$ and $\lambda_d = 0.04$ for Mode 2.

The results of this analysis are shown in Fig. 2–4. Fig. 2 shows a plot of the absolute value of the differences of the nondimensional damaged and nondimensional undamaged mode shapes (i.e., $\left|\Psi_n(\xi) - \Psi_{o,n}(\xi)\right|$) for all three damage scenarios and both modes; Fig. 2(a) shows the results for Mode 1 while Fig. 2(b) displays Mode 2 results. For convenience, the extent of the damage zone is indicated by the dash-dot lines on each plot. A logarithmic scale is used for the vertical axes due to the range of magnitudes involved. The results indicate that, even for the large damage case ($\delta = 0.3$), the changes in the mode shapes were rather small in magnitude. The sizes of the mode shape changes do appear to be proportional to the level of damage, as each order of magnitude increase in δ produced roughly an order of magnitude increase in the size of the differences. However, the differences themselves were at least two orders of magnitude smaller than the size of the mode shape for large levels of damage and at least four orders lower for small damage. This would indicate a fairly low level of sensitivity to damage (or at least damage modeled as indicated above). It can also be seen that maximum differences in magnitude did not necessarily occur within the damage zone, from which we conclude that the effect of damage on mode shapes (to the extent that it occurs) is not necessarily confined to the damage zone but can "leak out" to the rest of the mode. This low level of sensitivity to damage as well as the "leaking" of damage effects makes it difficult to uniquely determine the damage location, let alone characterize its magnitude. These results are consistent with the conclusions of several researchers that mode shape changes are poor indicators of damage.

Figs. 3(a) and (b) show the results of analyzing the modal curvature differences (i.e., $\left|\Psi''_n(\xi) - \Psi''_{o,n}(\xi)\right|$) in which several interesting features can be seen. (In this and all subsequent equations, a prime refers to a derivative with respect to the indicated independent variable.) First, we note that the effect of the damage on the modal curvatures was most significant within the damage zone; modal curvature changes here were approximately one to two orders of magnitude greater than in the rest of the beam for both modes. Thus, the most prominent modal curvature changes due to damage appear to be spatially well-localized, which is an important feature for any damage indicator. As was true for the mode shapes, the levels of curvature change increased essentially in proportion to the level of damage. Finally, sensitivity to damage (as indicated by the peak value of modal curvature change) was greater than what was observed for mode shape changes, although small levels of damage still produced fairly small curvature changes. These results lead us to conclude that modal curvatures offer an improved ability to locate damage as compared to mode shape changes; again, this is again consistent with results from the literature. However, the sensitivity of modal curvature changes to small damage levels (and, to a lesser extent, moderate damage levels) still appears to be somewhat low.

The analysis of modal fourth derivative changes (i.e., $\left|\Psi''''_n(\xi) - \Psi''''_{o,n}(\xi)\right|$) can be found in Figs. 4(a) and (b). Many of the features observed in Fig. 3 were also observed in these figures, including a well-localized

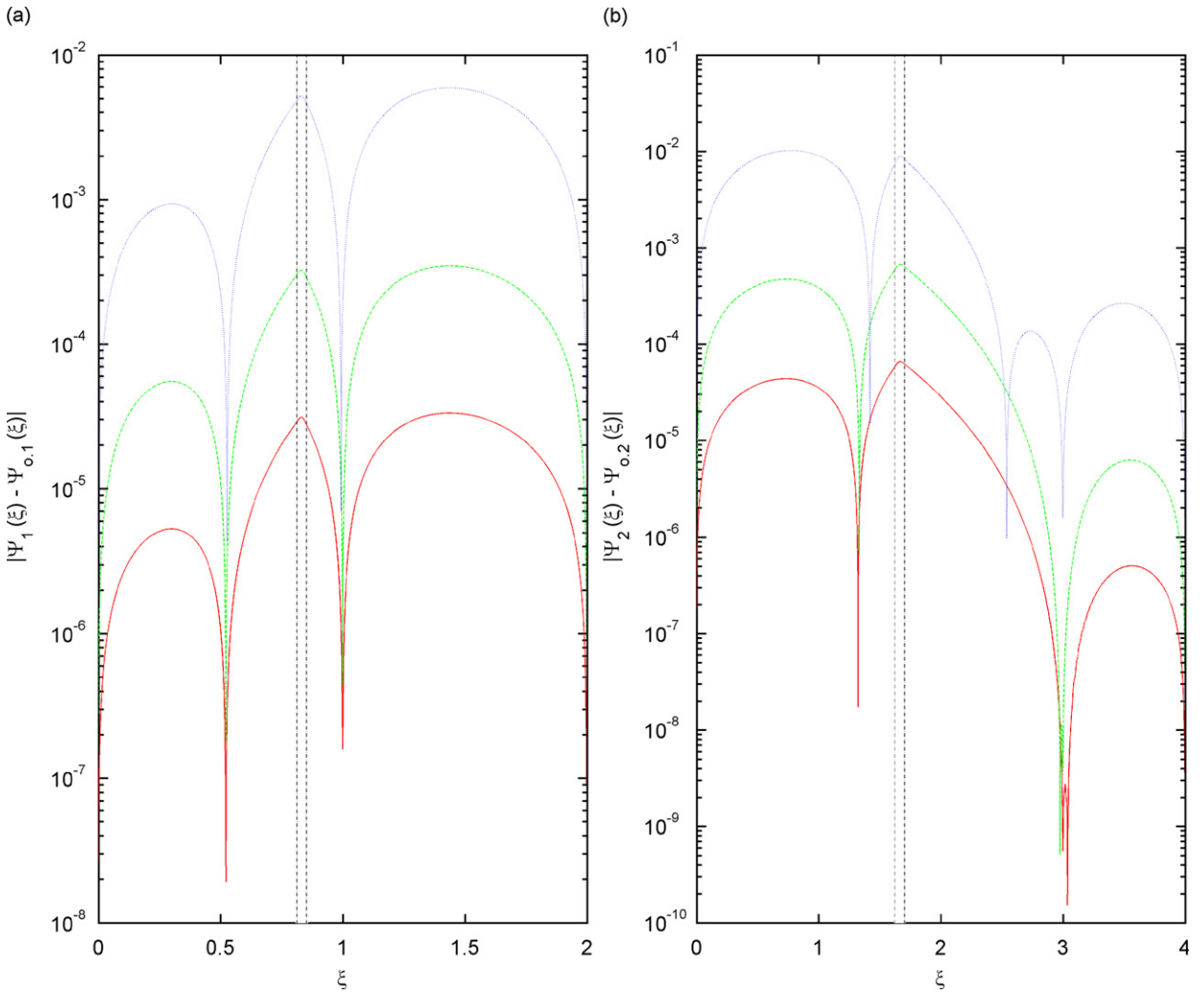

Fig. 2. Absolute value of the difference between damaged and undamaged nondimensional mode shapes due to changes in damage level. —— $\delta = 0.003$, — — — $\delta = 0.03$, · · · $\delta = 0.3$, — · — damage zone. (a) Mode 1, (b) Mode 2.

indication of the damage and close proportionality between the level of damage and the magnitude of the fourth derivative change. Also worth noting is the increased sensitivity to damage, as evinced by the large peak values of the derivative changes, even for the "small" damage case. Thus, modal fourth derivative changes also appear to be good candidates for use in damage identification. Note that the performance of modal derivative changes in the presence of noise and other error sources is not considered here—the question of robustness will be pursued in future work.

3.1.3. *Effect of damage zone size*

Next, we considered the influence of damage zone size on the modal properties. We assumed "small" damage, using the representative value of $\delta = 0.003$ for the maximum loss of depth. (Thus, $\mu = 0.003$ and $\kappa \approx 0.008973$ are the mass and stiffness loss parameters, respectively.) We again considered the first two modes of vibration only and examined three scenarios for the damage zone size: $l_d = 3$, 30, and 300. Thus, the values of λ_d are $\lambda_d = 0.005$, 0.05 and 0.5 for Mode 1 and $\lambda_d = 0.01$, 0.1 and 1.0 for Mode 2.

Figs. 5–7 summarize the results of this study. In each figure, the size of the damage zone is indicated by appropriate vertical lines. We first note, in Fig. 5, that the size of the damage zone had relatively little influence

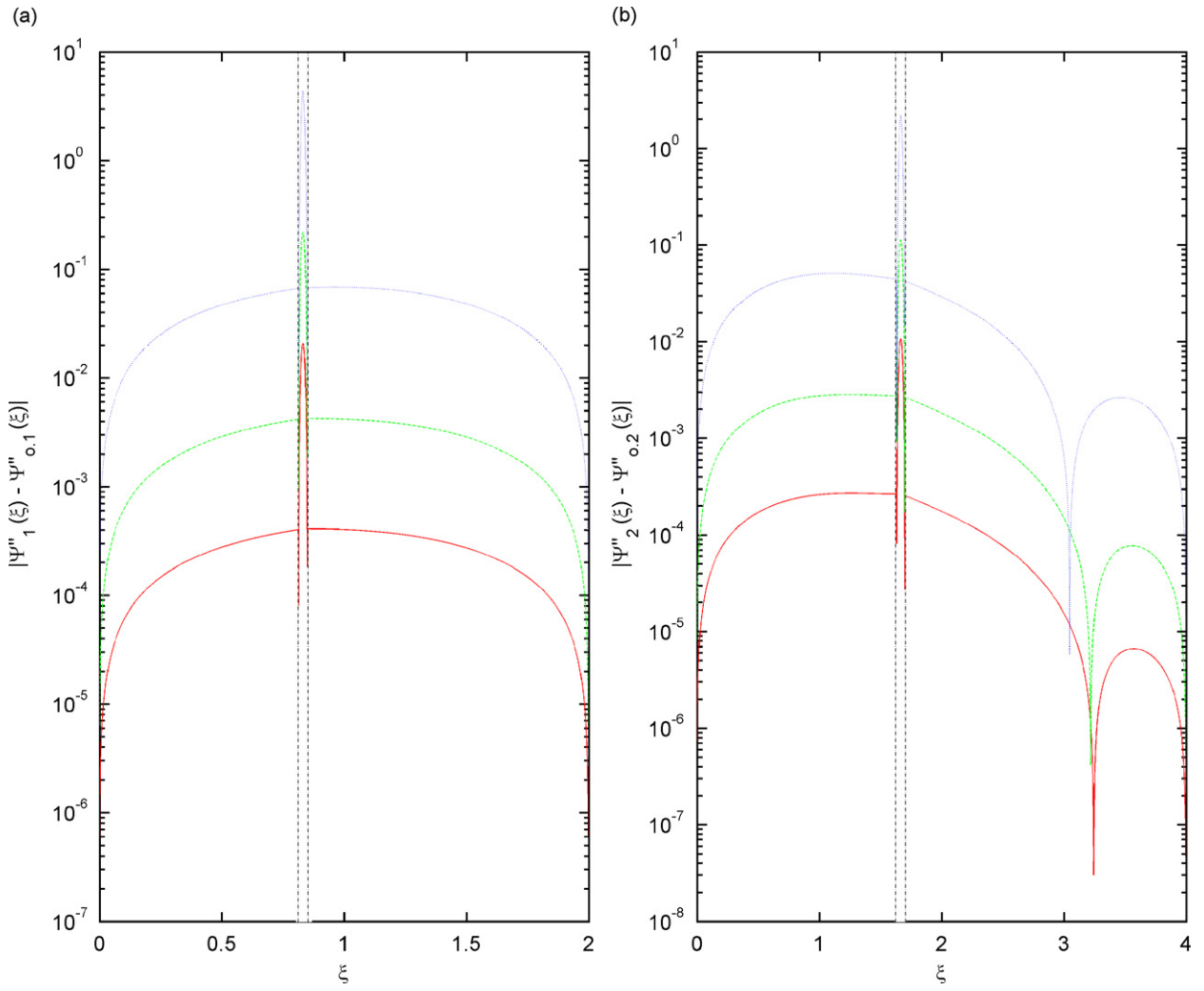

Fig. 3. Absolute value of the difference between damaged and undamaged nondimensional modal curvatures due to changes in damage level. —— $\delta = 0.003$, — — — $\delta = 0.03$, · · · $\delta = 0.3$, — · — damage zone. (a) Mode 1, (b) Mode 2.

upon the behavior of the mode shape changes other than to cause modifications in the overall magnitude of the changes. (This conclusion is not completely supported by the $\lambda_d = 1.0$ case in Fig. 5(b), although the behavior of $|\Psi_2(\xi) - \Psi_{o,2}(\xi)|$ for $0 \leqslant \xi \leqslant 0.6667$ is consistent with the conclusion.) In all cases presented, the sizes of the mode shape changes were rather small and showed no clear localization within the indicated damage zone. Each order of magnitude increase in the size of λ_d, however, caused an order of magnitude change in the levels of $|\Psi_n(\xi) - \Psi_{o,n}(\xi)|$, leading us to hypothesize that the latter quantity is directly proportional to λ_d.

When the changes in modal curvatures were considered, however, some new trends were discovered. Fig. 6 shows that well-localized changes in $|\Psi''_n(\xi) - \Psi''_{o,n}(\xi)|$ occurred when the damage zone was small or moderately sized, but the changes were not well localized for the large damage zone. Values of $|\Psi''_n(\xi) - \Psi''_{o,n}(\xi)|$ outside of the relevant damage zones appeared to behave in a manner quite similar to that observed for the mode shape changes, i.e., small values that are roughly proportional to the size of λ_d. However, sharp rises in magnitude change were found within the damage zones when the damage zone size was not large. Even more interestingly, the peak values of $|\Psi''_n(\xi) - \Psi''_{o,n}(\xi)|$ were approximately equal across all of the cases considered—the values ranged from 0.83×10^{-2} (Mode 2, $\lambda_d = 1.0$) to 2.12×10^{-2}

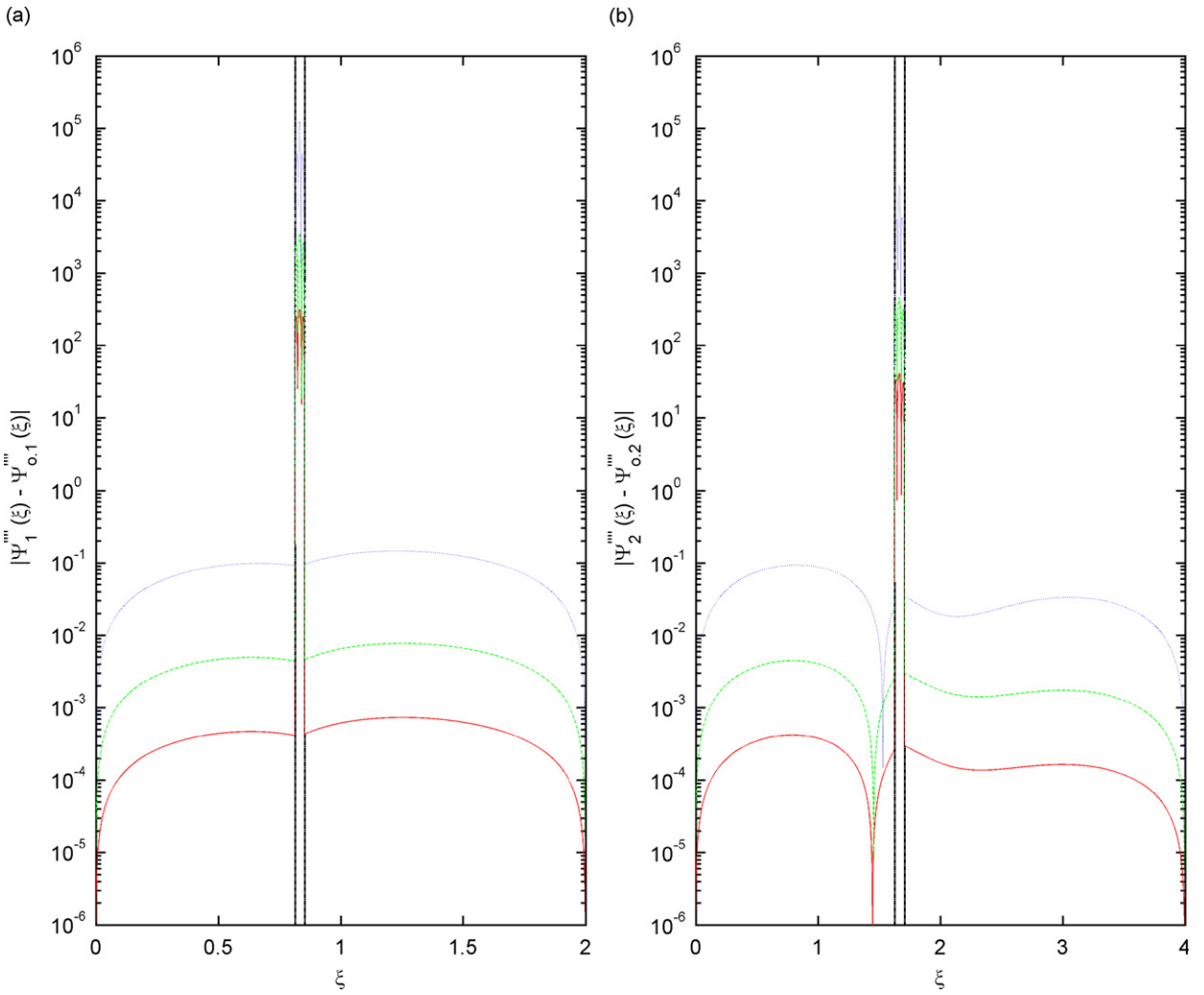

Fig. 4. Absolute value of the difference between damaged and undamaged modal nondimensional fourth derivatives due to changes in damage level. —— $\delta = 0.003$, — — — $\delta = 0.03$, · · · $\delta = 0.3$, — · — damage zone. (a) Mode 1, (b) Mode 2.

(Mode 1, $\lambda_d = 0.005$). Thus, damage zone sizes seem to affect modal curvatures in distinct ways inside versus outside of the damage zone: curvature changes appear to be small but directly proportional to λ_d outside of the damage zone, whereas they are larger but roughly independent of λ_d within the damage zone.

Finally, Fig. 7 reveals equally interesting behaviors in the modal fourth derivative changes due to damage. In this situation, the damage effect appeared to be well localized for all cases considered, including the "large" damage zone cases. Behaviors of $\left|\Psi''''_n(\xi) - \Psi''''_{o,n}(\xi)\right|$ outside of the damage zones followed the pattern of small values and direct proportionality to λ_d, but behaviors within the damage zones were noticeably different. Of particular interest is the observation that the smallest damage zone cases produced the largest peak values of $\left|\Psi''''_n(\xi) - \Psi''''_{o,n}(\xi)\right|$, suggesting an inverse proportionality to λ_d. This idea was further supported by the fact that each order of magnitude increase in λ_d produced a roughly two order of magnitude decrease in peak values of $\left|\Psi''''_n(\xi) - \Psi''''_{o,n}(\xi)\right|$. Thus, we hypothesize that the largest values of the modal fourth derivative changes should be inversely proportional to λ_d^2, which implies that these quantities should be particularly sensitive to damage of small spatial extent. This feature is quite desirable for a damage indicator, so its use in structural health monitoring seems promising. Further features of the modal fourth derivative must be determined, however, before it can be deemed acceptable for this purpose.

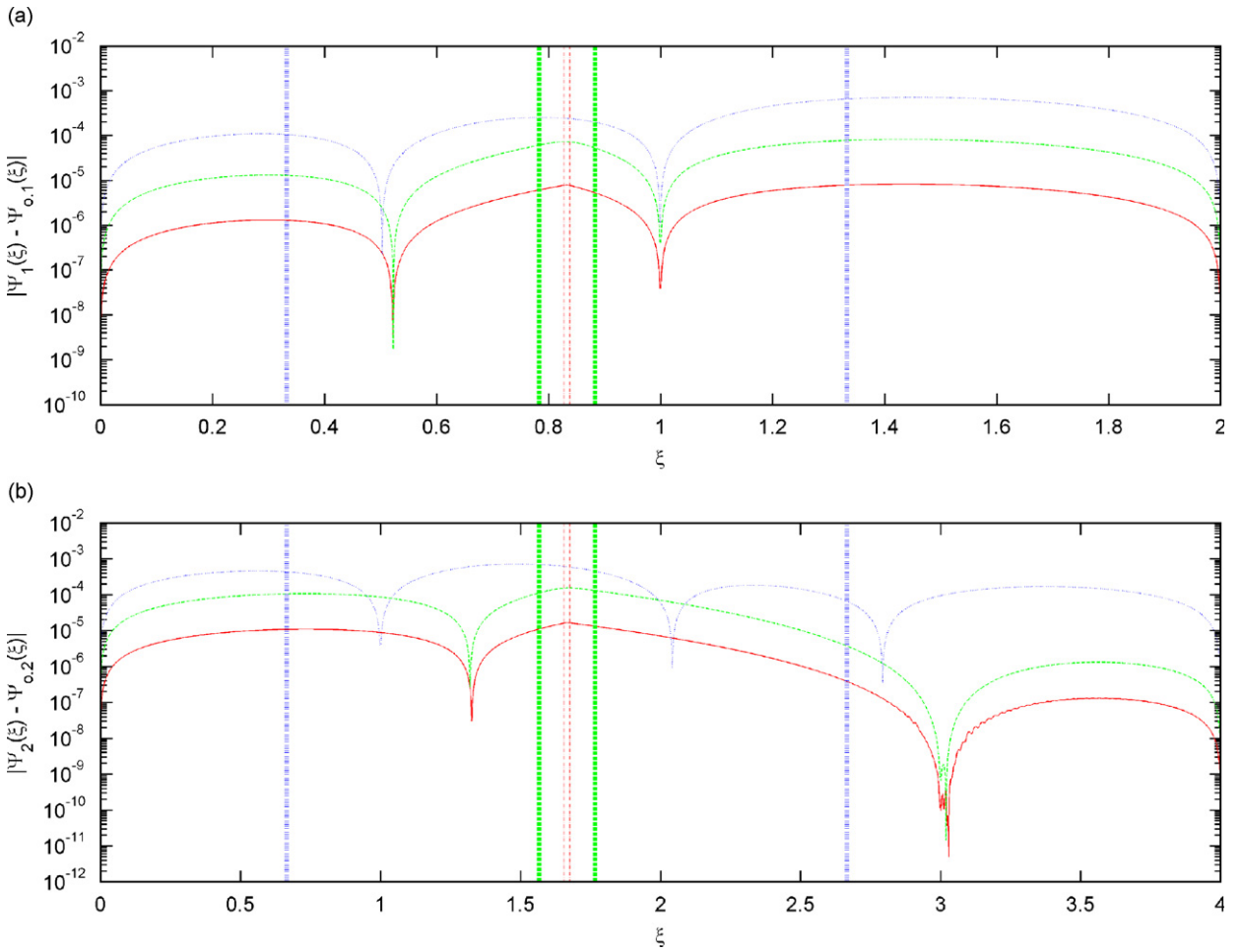

Fig. 5. Absolute value of the difference between damaged and undamaged nondimensional mode shapes due to changes in damage zone size. —— $\lambda_d = 0.01$, — · — damage zone for $\lambda_d = 0.01$, — — — $\lambda_d = 0.1$, — — — damage zone for $\lambda_d = 0.1$, · · · $\lambda_d = 1.0$, ▪ ▪ ▪ damage zone for $\lambda_d = 1.0$. (a) Mode 1, (b) Mode 2.

3.1.4. *Influence of damage model*

In this section, we explore the influence of the damage model on the modal response. To this end, we again used the simplified damage model indicated in Eq. (13), but we varied the parameter k in the loss of depth function shown in Eq. (14) so as to change the rate by which the depth varies within the damage zone. The resulting stiffness modification functions are shown in Fig. 8 for various values of k. We chose three values of k for this study: $k = 1$, 2, and 4. We note that increasing k expands the range of values within the damage zone for which the stiffness modification function stays close to unity. Since $\Delta(\eta)$ is required to go to zero at the edges of the boundary zone, this behavior leads to a more abrupt variation from fully damaged to undamaged as k increases. These effects reveal themselves most dramatically in the variations of $\Delta'(\eta)$ and $\Delta''(\eta)$ with k, shown in Fig. 9. We observe that larger k values result in very large values of $\Delta'(\eta)$ and $\Delta''(\eta)$ near the edges of the damage zone, particularly for $\Delta''(\eta)$. Recall that $\Delta(\eta)$ also depends upon the assumed level of damage δ; we used $\delta = 0.025$ for our analysis. (Similar results were observed when other levels of damage were used.) As for the mass modification function, we set $\mu = \delta$ and fixed $\Gamma(\eta) = H(\eta + 1) - H(\eta - 1)$, where $H(\cdot)$ is the Heaviside step function. This choice is not, strictly speaking, consistent with the simplified damage model, as it "decouples" the variations in mass from the variations in stiffness. We chose to not vary $\Gamma(\eta)$ so as to concentrate upon stiffness modification effects. Note that our choice of $\Gamma(\eta)$ maximizes the possible effects on mass loss on the mode shapes and their derivatives.

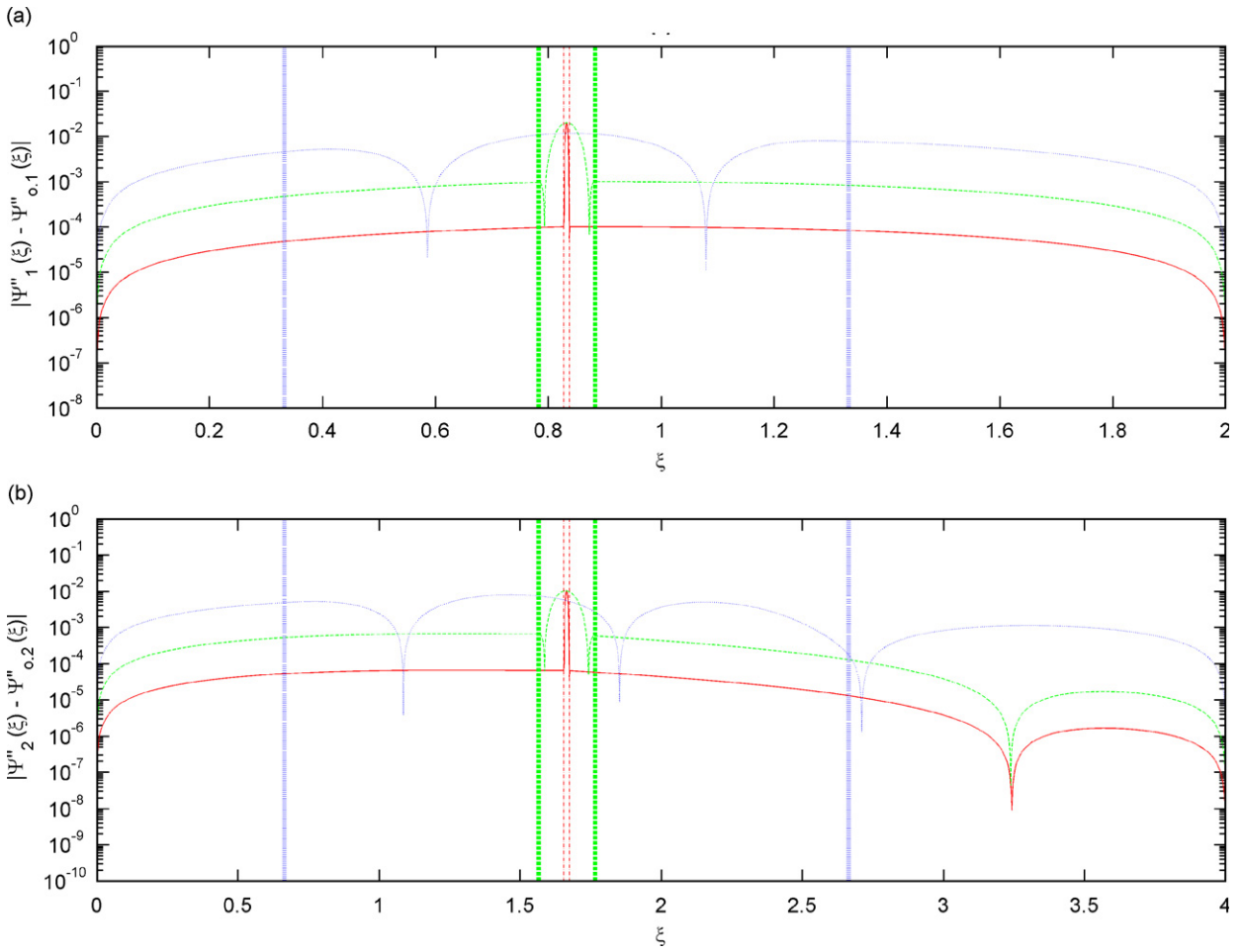

Fig. 6. Absolute value of the difference between damaged and undamaged nondimensional modal curvatures due to changes in damage zone size. —— $\lambda_d = 0.01$, — · — damage zone for $\lambda_d = 0.01$, — — — $\lambda_d = 0.1$, — — — damage zone for $\lambda_d = 0.1$, · · · $\lambda_d = 1.0$, ▪ ▪ ▪ damage zone for $\lambda_d = 1.0$. (a) Mode 1, (b) Mode 2.

In our studies, we chose to consider Mode 1 only, and we fixed the damage location and damage radius to be $\xi_d = \frac{5}{6}$ and $\lambda_d = \frac{1}{6}$. In Fig. 10, we plot the changes in second derivative, third derivative, and fourth derivative of the first mode shape for varying values of k, showing a closer view of the damage zone. Note that we are not plotting the absolute value of the changes in these derivatives but rather the actual difference. An extremely interesting result is observed when Fig. 10 is compared to the stiffness modification function and its derivatives (as shown in Figs. 8 and 9). In Fig. 10(a), we note that the behavior of the change in second derivative due to damage is quite similar to that of the stiffness modification function as k is varied. That is to say, as k was increased, the quantity $\Psi''_1(\xi) - \Psi''_{o,1}(\xi)$ changed from being sharply peaked in the center of the damage zone to making a more abrupt transition at the edges of the damage zone. In Fig. 10(b), we observe that the behavior of $\Psi'''_1(\xi) - \Psi'''_{o,1}(\xi)$ mimicked that of $\Delta'(\eta)$ as k was changed, with the peak values moving closer to the edges of the damage zone with increasing k. Finally, Fig. 10(c) displays a strong correlation between $\Psi''''_1(\xi) - \Psi''''_{o,1}(\xi)$ and $\Delta''(\eta)$. Most notably, the locations of the large peaks observed in $\Psi''''_1(\xi) - \Psi''''_{o,1}(\xi)$ appear to correspond quite well to the locations of peak values of $\Delta''(\eta)$. These results strongly suggest that there is a relationship between the $(n-2)$th derivative of the stiffness modification function and changes in the nth modal derivative. One caveat, however, must be applied to this observation. A careful examination of Fig. 10 shows that the modal derivative changes are not exactly proportional to $\Delta(\eta)$ or its derivatives; Fig. 10(a), for example, shows a clear modulation of the second derivative change in regions where $\Delta(\eta)$ is

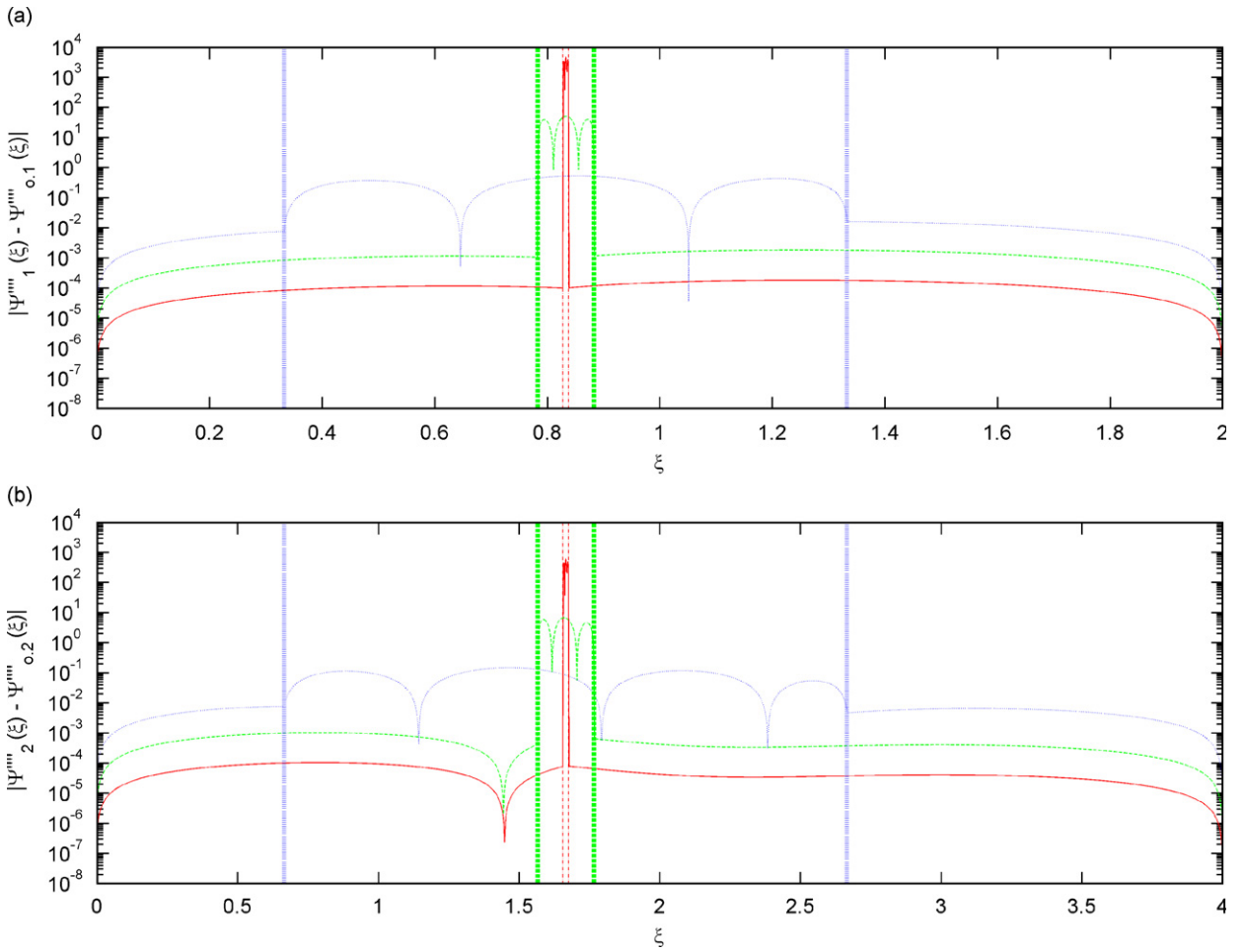

Fig. 7. Absolute value of the difference between damaged and undamaged modal nondimensional fourth derivatives due to changes in damage zone size. —— $\lambda_d = 0.01$, — · — damage zone for $\lambda_d = 0.01$, — — — $\lambda_d = 0.1$, — — — damage zone for $\lambda_d = 0.1$, · · · $\lambda_d = 1.0$, ▪ ▪ ▪ damage zone for $\lambda_d = 1.0$. (a) Mode 1, (b) Mode 2.

effectively "flat". Thus, other factors must be at work to produce the overall behavior of the modal derivative changes.

3.1.5. *Effect of mass modeling*

As mentioned previously, it is not common for researchers to give much consideration to mass modeling in their investigations. Researchers are often explicitly considering cracks as the source of damage, which is associated with very little mass loss. However, other loss mechanisms, such as corrosion or impact damage, can have noticeable mass loss, which conceivably could affect the behavior of the modal changes. To see whether or not this idea is justified, we chose to study the effect of different mass loss models on the higher order modal derivatives. We once again employed the simplified damage model described by the Eqs. (13) and (14) but, similar to the procedure of Section 3.1.4, we decoupled the variation of the stiffness modification function from that of the mass modification function by fixing $k = 1$ when calculating $\Delta(\eta)$ but using various k values when determining $\Gamma(\eta)$. Note that as $k \to \infty$, the mass modification function $\Gamma(\eta) \to H(\eta + 1) - H(\eta - 1)$, a situation we labeled as the "full mass loss" limit; $k \to 0$ leads to $\Gamma(\eta) \approx 0$, which we refer to as the "no mass loss" limit.

Fig. 11 shows the results of varying the mass loss model on the changes in mode shapes and modal derivatives under the assumption of top and bottom through-thickness cracks. More specifically, we considered both first

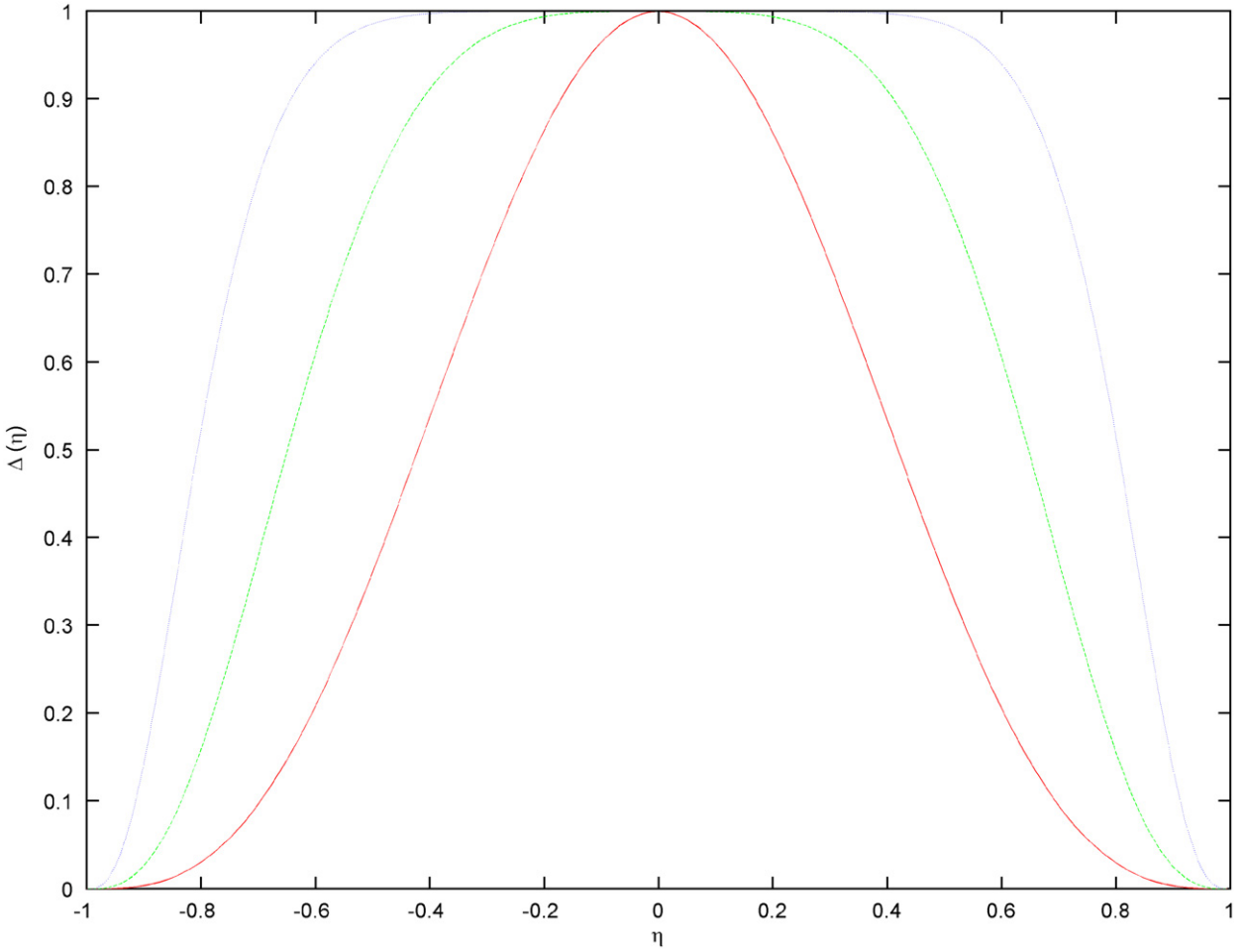

Fig. 8. Various stiffness modification functions for the simplified damage model with $\delta = 0.025$ and $\Xi(\eta) = \cos^3((\pi/2)|\eta|^k)$, $|\eta| \leqslant 1$. —— $k = 1$, – – – $k = 2$, · · · $k = 4$.

mode and fifth mode vibration of the beam, for which we have $\Lambda = 2$ and $\xi_d = 0.83333$ (Mode 1) and $\Lambda = 10$ and $\xi_d = 4.16667$ (Mode 5). The damage radius was set to 40 units, leading to $\lambda_d = 0.06667$ for Mode 1 and $\lambda_d = 0.33333$ for Mode 5. The damage level was taken as $\delta = 0.30$, resulting in $\mu = 0.30$ and $\kappa = 0.657$. Shown in this figure are the resulting changes in modal displacements, curvatures, and fourth derivatives of the damaged beam for both modes. Mode 1 showed almost no sensitivity to the choice of mass model, with only small variations in mode shape changes. Mode 5 had a somewhat higher level of sensitivity to mass model choice, as evinced by the wider range of mode shape and modal curvature changes, although this sensitivity diminished as the derivative order increased. Similar behaviors are observed in Fig. 12 when a lower damage level was used. In this case, we lowered the damage scales to $\delta = \mu = 0.03$ and $\kappa = 0.087327$. In fact, the variations are almost identical to those seen in Fig. 11, although the overall scale is lower.

Next, we switched our crack modeling assumption to through-thickness cracks in the middle of the section. We chose to study the same vibration modes, damage locations, and damage radii as the previous cases, but the loss parameters were modified to reflect the change in damage geometry. It can be shown that, while $\mu = \delta$ still holds, the stiffness loss parameter relates to the loss of section parameter as $\kappa = \delta^3$. Thus, the high damage level case gives us $\mu = 0.30$ and $\kappa = 0.027$, while the moderate damage scenario has $\mu = 0.03$ and $\kappa = 2.7 \times 10^{-5}$. Hence, mass loss scales are larger than the corresponding stiffness loss scales under this damage assumption. Figs. 13 ($\delta = 0.30$) and 14 ($\delta = 0.03$) are the equivalents of Figs. 11 and 12 for this mid-section crack situation. There is an overall greater sensitivity to mass modeling present in this case; even

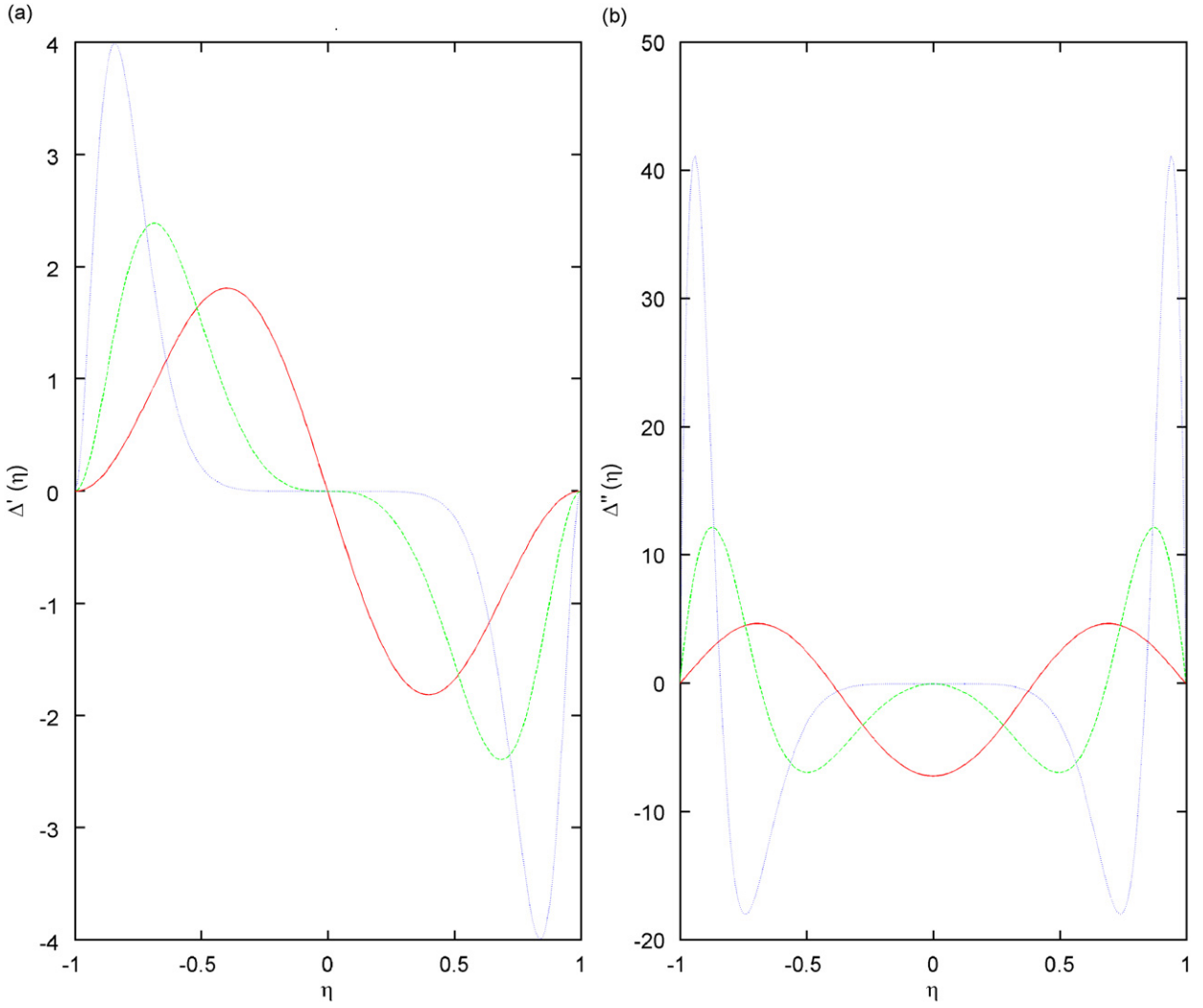

Fig. 9. Derivatives of the various stiffness modification functions. —— $k=1$, — — — $k=2$, · · · $k=4$. (a) $\Delta'(\eta)$, (b) $\Delta''(\eta)$.

the fourth order modal derivative changes show some influence due to mass modeling. While the main effect of changing the mass model appears to be a simple modulation in the amplitudes of the damage-induced changes, there are some examples of minor variations in spatial trends (e.g., the appearance of the small downward peak in $\Psi''_5(\xi)-\Psi''_{o,5}(\xi)$ as k tends towards infinity) resulting from mass model changes. Thus, mass modeling choices appear to be more important for the damage scenario of mid-section cracking than is true for the top/bottom crack scenario. This idea will be explored in more detail in Section 3.2.2.

3.2. Cantilevered beam problem

3.2.1. Effect of damage location

The next problem considered was that of a cantilevered beam with damage. Fig. 15 shows the relevant details; in this case, we do not specify a fixed location for the damage zone. The nondimensional form of the undamaged modal solutions is

$$\Psi_{o,n}(\xi)=A_n\left[\left(\cos\frac{\pi\Lambda_n}{2}+\cosh\frac{\pi\Lambda_n}{2}\right)\left(\sin\frac{\pi\xi}{2}-\sinh\frac{\pi\xi}{2}\right)-\left(\sin\frac{\pi\Lambda_n}{2}+\sinh\frac{\pi\Lambda_n}{2}\right)\left(\cos\frac{\pi\xi}{2}-\cosh\frac{\pi\xi}{2}\right)\right], \quad (15)$$

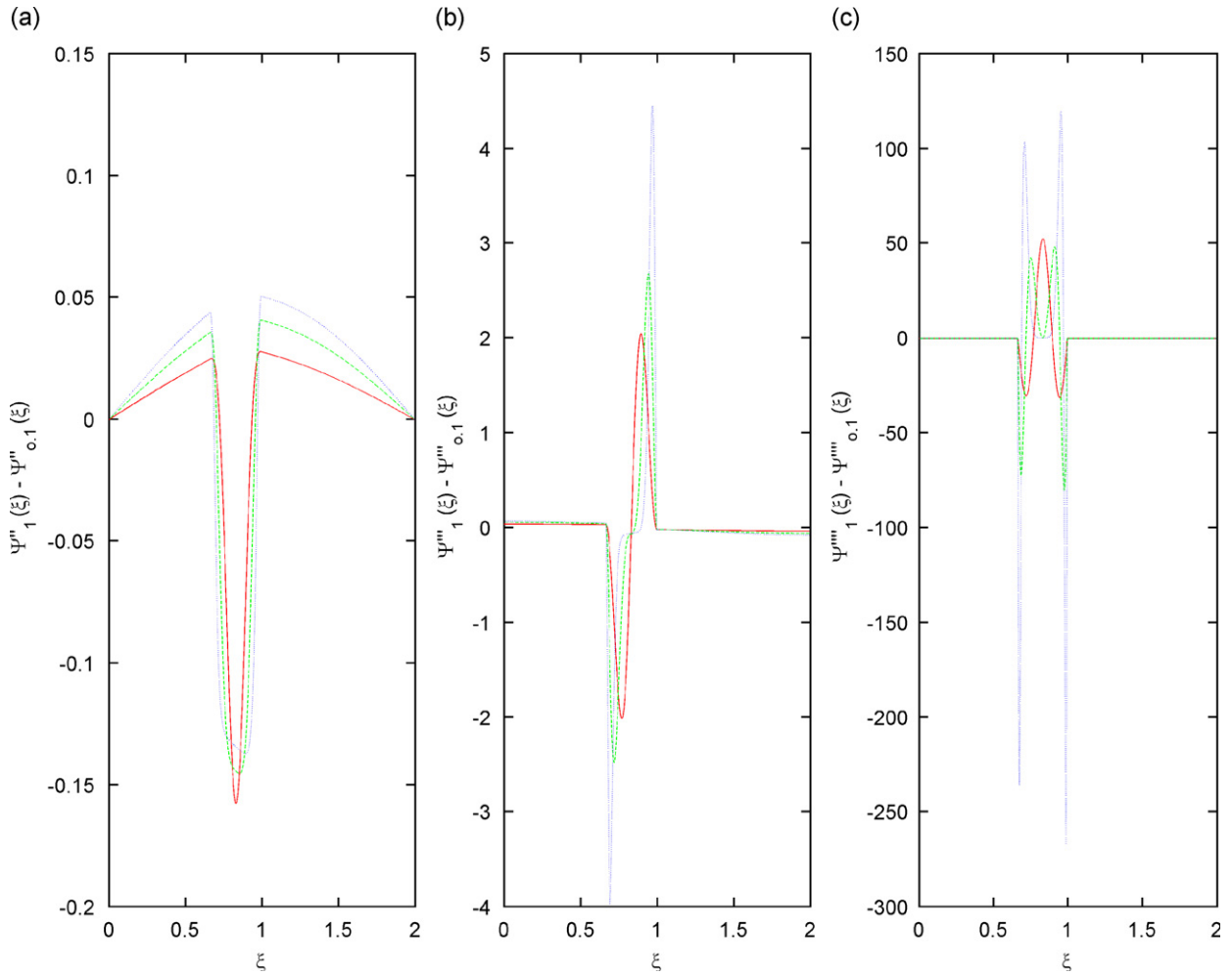

Fig. 10. Difference between damaged and undamaged nondimensional first mode properties due to changes in stiffness modification function. —— $k=1$, — — — $k=2$, · · · $k=4$. (a) second derivative, (b) third derivative, (c) fourth derivative.

where the amplitude coefficient $A_n = \left(2\tanh(\pi\Lambda_n/2) - 2\tan(\pi\Lambda_n/2)\right)^{-1}$. (Note that this solution normalizes the tip displacement for each mode.) The values of Λ_n must satisfy the condition $\cos(\pi\Lambda_n/2)\cosh(\pi\Lambda_n/2) = -1$ arising from the eigenvalue problem for cantilevered beam vibration. (See Ref. [21] for details.) It can be shown that, for sufficiently large values of n, $\Lambda_n \approx 2n-1$ is a reasonable approximation for the nondimensional beam length.

Solutions of the cantilevered beam problem display the same properties as discussed in Section 3.1 for the simply supported beam; for sake of brevity, specific results are not shown. One property that can be studied more systematically using the cantilevered beam problem is the influence of damage location on modal behaviors. To do so, we considered Mode 2 vibrations of the beam. The nondimensional length of the beam for this mode is $\Lambda_2 = 2.9884$; we assumed a fixed nondimensional damage zone radius of $\lambda_d = 0.05$ and used the Eq. (13) damage model with $k=1$ and a damage level of $\delta = 0.03$. (The stiffness loss and mass loss parameters are $\kappa \approx 0.08733$ and $\mu = 0.03$, as previously computed in Section 3.1.2 for the "moderate" damage case.)

Fig. 16 summarizes results obtained for this study, in which six separate damage locations ($\xi_{d1} = 2.34$, $\xi_{d2} = 1.40$, $\xi_{d3} = 0.65$, $\xi_{d4} = 1.58$, $\xi_{d5} = 0.06$, and $\xi_{d6} = 2.94$) were specified across the beam. Damage locations at the ends of the beam were shifted inwards in order to prevent interactions between the damage

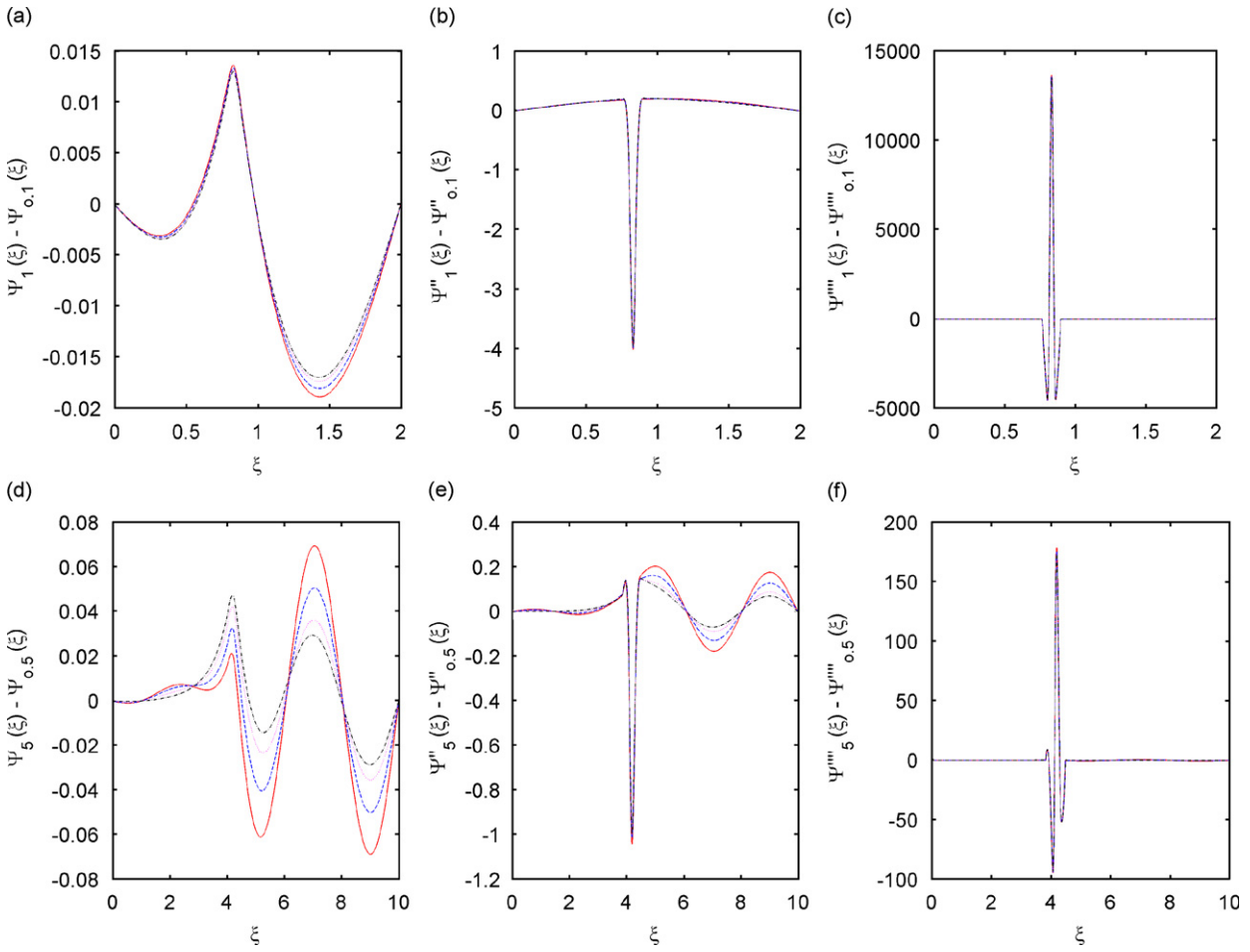

Fig. 11. Difference between damaged and undamaged nondimensional modal properties for various mass loss models and top-bottom through-thickness cracks with high damage levels. —— $k=0$, — — — $k=1$, · · · $k=4$, — · — $k=\infty$. (a) Mode 1 shape, (b) Mode 1 curvature, (c) Mode 1 fourth derivative, (d) Mode 5 shape, (e) Mode 5 curvature, (f) Mode 5 fourth derivative.

zones and the boundaries. The basis for selecting these points is that each one is a location at which either the second mode or one of the second mode derivatives is approximately equal to zero. In particular, $\Psi_{o,2}(\xi) \approx 0$ for $\xi = \xi_{d1}$ and ξ_{d5}, $\Psi'_{o,2}(\xi) \approx 0$ for $\xi = \xi_{d2}$ and ξ_{d5}, $\Psi''_{o,2}(\xi) \approx 0$ for $\xi = \xi_{d3}$ and ξ_{d6}, and $\Psi''''_{o,2}(\xi) \approx 0$ for $\xi = \xi_{d4}$ and ξ_{d6}. (The approximations are less accurate for $\xi = \xi_{d5}$ and ξ_{d6} due to the shifts away from the boundaries.) In Fig. 16(a), we see that changes in damage location did produce different effects upon the mode shape changes, although no clear trends in behavior were discerned. The overall magnitudes of the changes were small and not well localized spatially, as would be anticipated based upon the results of Section 3.1. The impact of varying damage location becomes much clearer, however, when Figs. 16(b) and (c) are studied. In these figures, the changes in modal curvature and modal fourth derivative have much better spatial localization, so the main impact of varying ξ_d can be seen as a noticeable variation in magnitudes of the resulting modal changes. The observed changes had their largest magnitudes for $\xi = \xi_{d5} = 0.06$, while more moderate changes were observed for $\xi = \xi_{d2} = 1.40$, $\xi = \xi_{d4} = 1.58$, and $\xi = \xi_{d1} = 2.34$. Finally, very small changes were associated with two damage locations, $\xi = \xi_{d3} = 0.65$ and $\xi = \xi_{d6} = 2.94$. In fact, the changes in modal behavior associated with ξ_{d6} are barely visible in Figs. 16(b) and (c), which contrasts significantly with the prominent change in mode shape seen in Fig. 16(a) when this damage location is used. Since the damage itself was identical across these six cases, these effects must be attributable solely to the influence of the location.

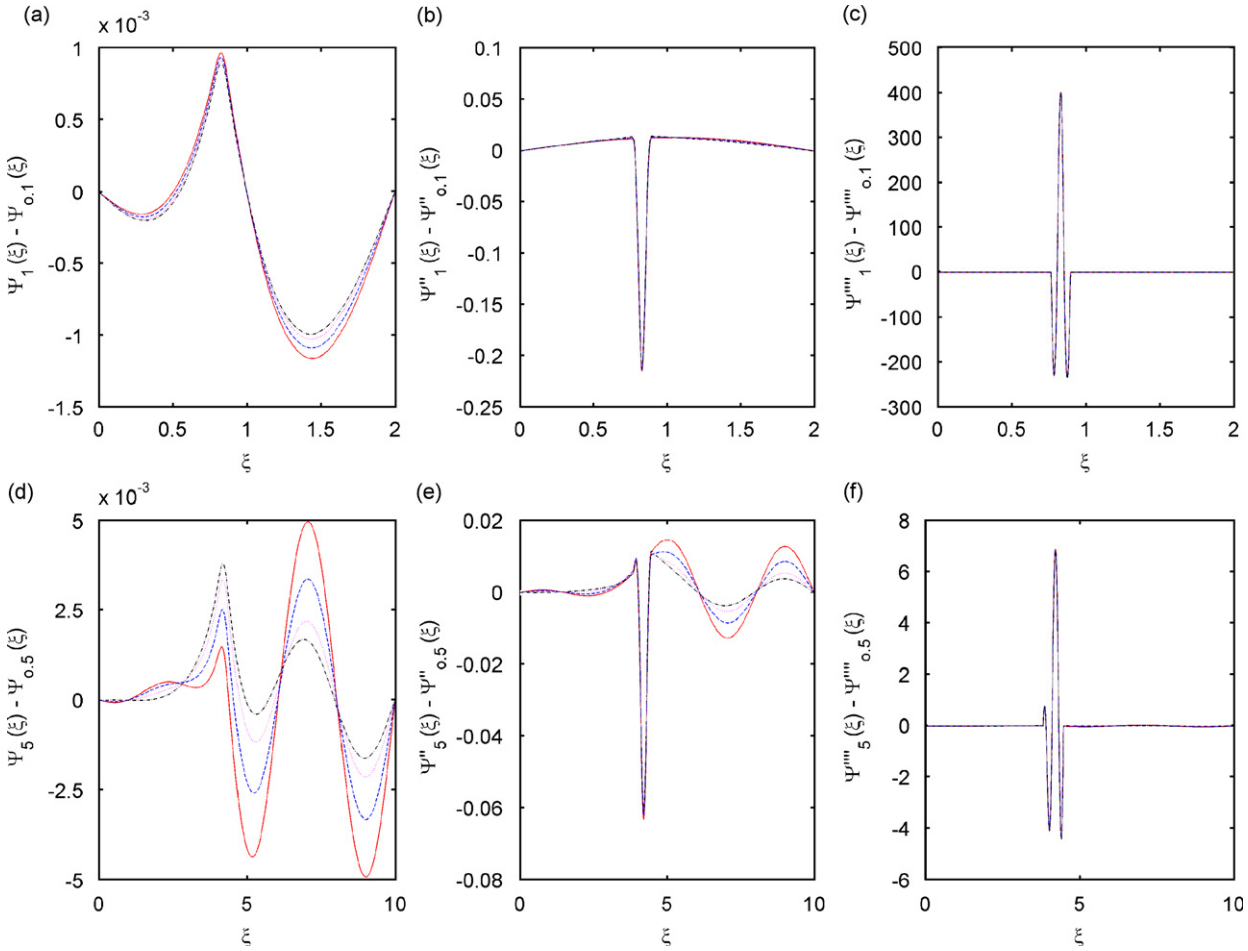

Fig. 12. Difference between damaged and undamaged nondimensional modal properties for various mass loss models and top-bottom through-thickness cracks with moderate damage levels. —— $k = 0$, — — — $k = 1$, · · · $k = 4$, — · — $k = \infty$. (a) Mode 1 shape, (b) Mode 1 curvature, (c) Mode 1 fourth derivative, (d) Mode 5 shape, (e) Mode 5 curvature, (f) Mode 5 fourth derivative.

The common feature of the two locations that indicated very low levels of damage (i.e., $\xi = \xi_{d3}$ and ξ_{d6}) is that the undamaged mode shape has nearly zero curvature at these points. Moreover, large values of the modal curvature (e.g., near $\xi = 0$) tend to correspond to large indications of damage in the second and fourth derivatives. Hence, we surmise that the underlying modal curvature of the beam plays an important role in determining sensitivity of the higher derivatives to damage. (While not shown here, it is worth noting that the third derivative displayed the same sort of behavior as observed in Figs. 16(b) and (c), while the modal slope changes were similar in nature to the mode shape changes seen in Fig. 16(a).) This relationship is emphasized in Fig. 17, in which six damage locations were chosen at roughly uniform spacing across the beam. (Again, damage locations near the ends of the beam are shifted inwards.) The damage scenario used in conjunction with Fig. 16 was utilized here. We plot the change in second mode modal curvature due to damage at each of these locations. In addition, a scaled version of the second derivative of the undamaged mode shape is plotted. (The scaling factor is κ, the stiffness loss coefficient. The reasons for this choice will be discussed in Section 4.) There is a very good level of agreement between the observed changes in modal curvature and the scaled modal curvature of the undamaged beam. Thus, this study strongly suggests that damaged-induced changes in the higher order modal derivatives are influenced by the underlying modal curvature of the undamaged system.

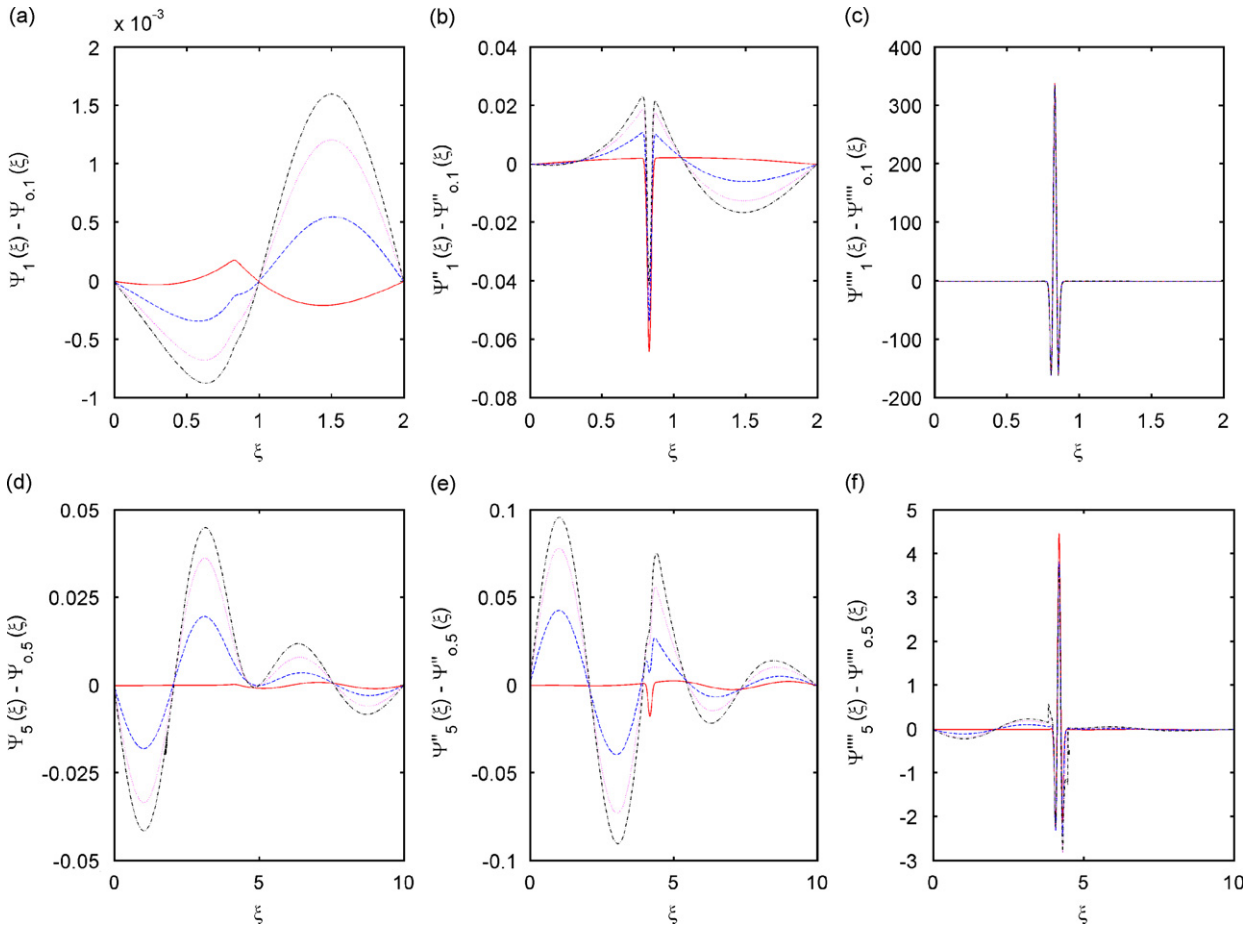

Fig. 13. Difference between damaged and undamaged nondimensional modal properties for various mass loss models and mid-section through-thickness cracks with high damage levels. —— $k=0$, – – – $k=1$, · · · $k=4$, – · – $k=\infty$. (a) Mode 1 shape, (b) Mode 1 curvature, (c) Mode 1 fourth derivative, (d) Mode 5 shape, (e) Mode 5 curvature, (f) Mode 5 fourth derivative.

3.2.2. *Magnitudes of governing equation terms*

In anticipation of the formal analyses to be discussed in Section 4, we now numerically investigate the magnitudes of the various terms that govern the behavior of the damaged mode shapes. Rather than studying Eq. (10), however, we define a function $\Phi_n(\xi) \equiv \Psi_n(\xi) - \Psi_{o,n}(\xi)$ that we call the "discontinuity" function. $\Phi_n(\xi)$ describes the damage-induced differences in the nondimensional mode shape. Introducing this function into Eq. (10) results in

$$\frac{\mathrm{d}^2}{\mathrm{d}\xi^2}\left[\{1-\kappa\Delta(\eta(\xi))\}\frac{\mathrm{d}^2\Phi_n(\xi)}{\mathrm{d}\xi^2}\right] - \left(\frac{\pi}{2}\right)^4\Omega_n^2\{1-\mu\Gamma(\eta(\xi))\}\Phi_n(\xi)$$
$$= \frac{\mathrm{d}^2}{\mathrm{d}\xi^2}\left[\kappa\Delta(\eta(\xi))\frac{\mathrm{d}^2\Psi_{o,n}(\xi)}{\mathrm{d}\xi^2}\right] + \left(\frac{\pi}{2}\right)^4\left[\Omega_n^2 - 1 - \mu\Omega_n^2\Gamma(\eta(\xi))\right]\Psi_{o,n}(\xi). \tag{16}$$

While this equation is more complicated than Eq. (10), the behavior of the component terms is more easily seen using Eq. (16). We designate the first and second term on the left-hand side of this equation as $T_1(\xi)$ and $T_2(\xi)$, respectively, while the first and second term on the right-hand side of the equation are labeled $T_3(\xi)$ and $T_4(\xi)$.

Numerical investigations of Eq. (16) for various combinations of parameters led to the identification of three distinct types of responses. These responses are illustrated in Fig. 18 for the problem of a cantilevered beam with a mid-section crack of damage level $\delta = 0.02$, resulting in $\mu = 0.02$ and $\kappa = 8.0 \times 10^{-6}$.

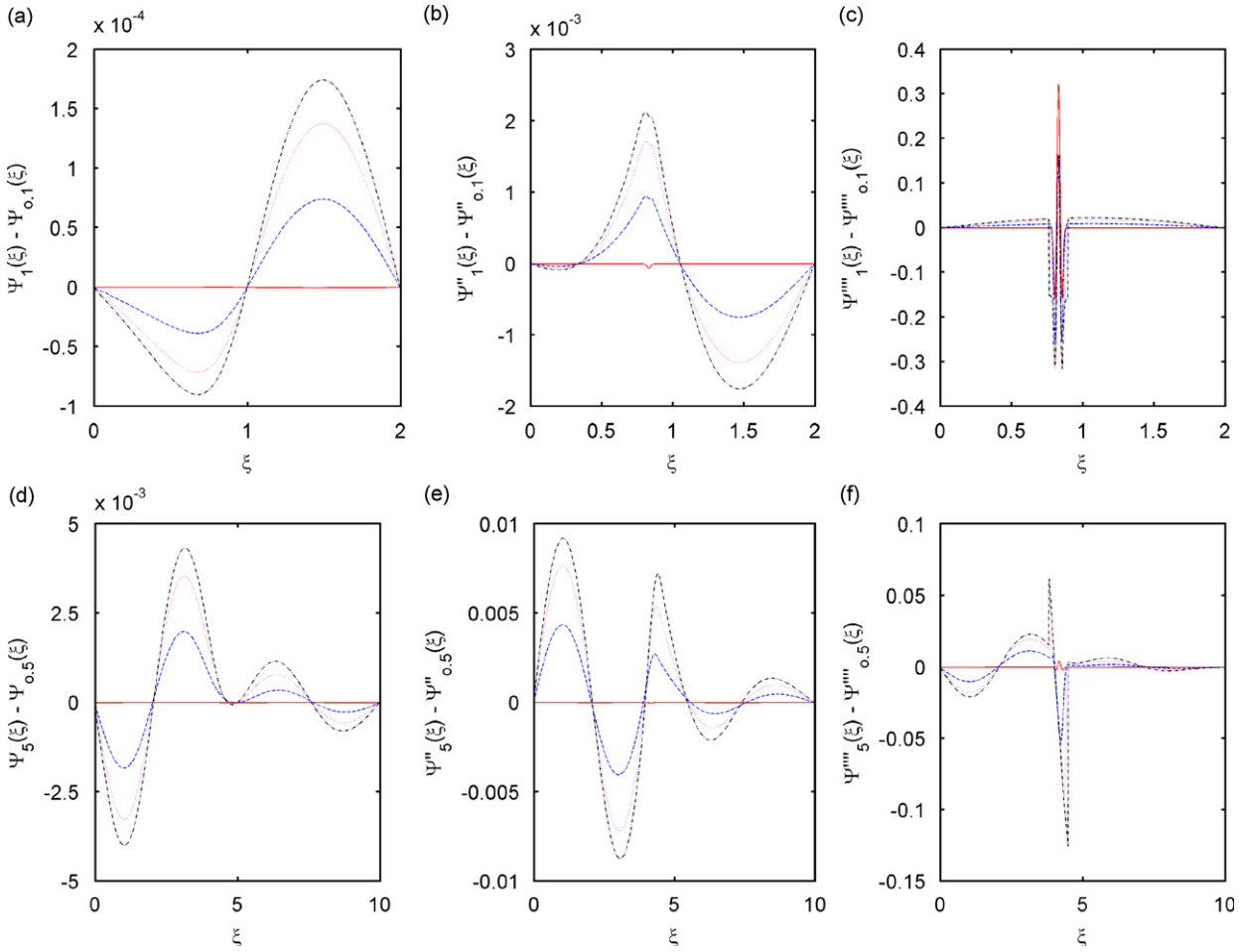

Fig. 14. Difference between damaged and undamaged nondimensional modal properties for various mass loss models and mid-section through-thickness cracks with moderate damage levels. —— $k=0$, — — — $k=1$, · · · $k=4$, — · — $k=\infty$. (a) Mode 1 shape, (b) Mode 1 curvature, (c) Mode 1 fourth derivative, (d) Mode 5 shape, (e) Mode 5 curvature, (f) Mode 5 fourth derivative.

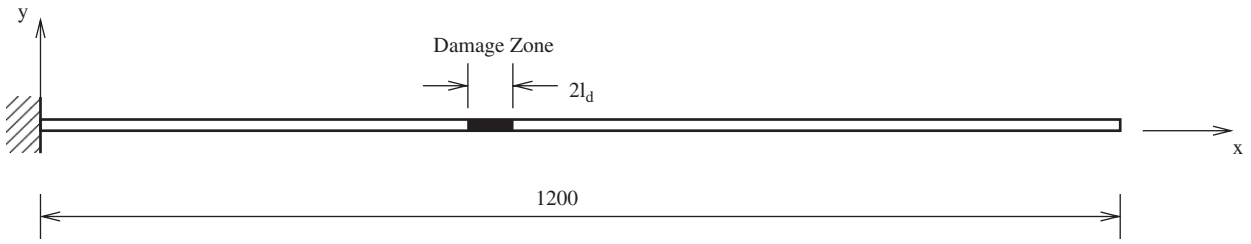

Fig. 15. The cantilevered beam problem.

(These results are representative of other damage scenarios as well.) We show results for Mode 1 vibration with $\Lambda_1 = 1.19373$, $\xi_d = 0.53111$, and varying damage radii λ_d. The simplified damage model was used with $k=1$ for the loss of section exponent.

For the first type of response, shown in Fig. 18(a) for the case $\lambda_d = 0.002$, $T_1(\xi)$ and $T_3(\xi)$ are nearly identical within the damage zone, and both of these terms are significantly larger than $T_2(\xi)$ and $T_4(\xi)$. While the degree to which $T_1(\xi)$ and $T_3(\xi)$ exceed $T_2(\xi)$ and $T_4(\xi)$ is very sensitive to the parameter values, what

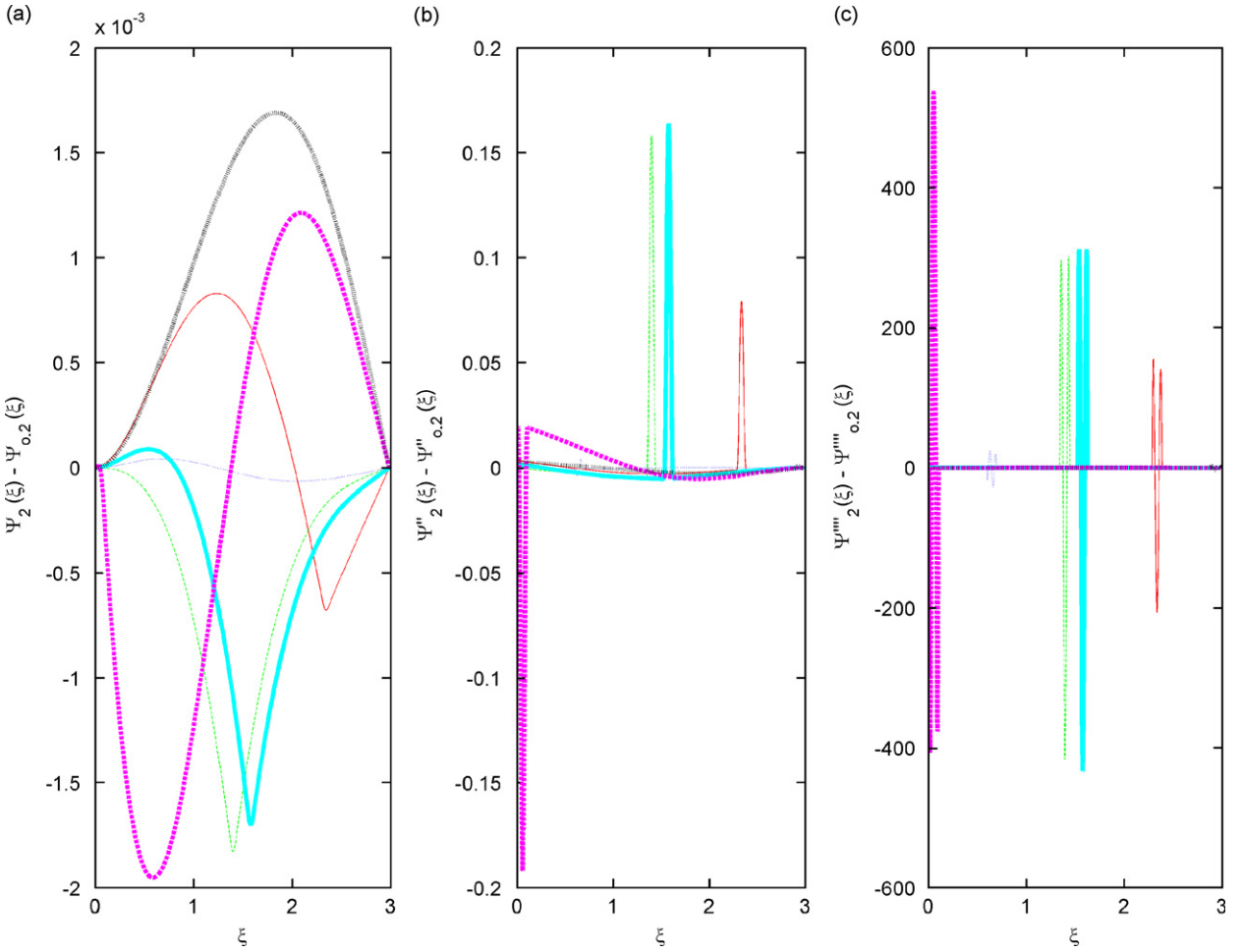

Fig. 16. Difference between nondimensional damaged and undamaged second mode properties due to changes in damage location. —— $\xi_d = 2.34$, — — — $\xi_d = 1.40$, · · · $\xi_d = 0.65$, ——— $\xi_d = 1.58$, — — — $\xi_d = 0.06$, ▪ ▪ ▪ $\xi_d = 2.94$. (a) mode shape, (b) modal curvature, (c) modal fourth derivative.

characterizes the behavior of this situation is the ability to neglect the changes in inertial effects that arise from $T_2(\xi)$ and $T_4(\xi)$ and assume that $T_1(\xi) \approx T_3(\xi)$, which involves only stiffness effects, completely determines the discontinuity function inside the damage zone. Because of this, we call this behavior "stiffness-dominated". Note that the magnitudes of $T_1(\xi)$ and $T_3(\xi)$ are fairly large compared to the scale of the damage; as a consequence, some derivative of the discontinuity function in the damage zone must also be large.

Fig. 18(c) shows the results for $\lambda_d = 0.2$, illustrating a second type of behavior. Here, it is now $T_1(\xi)$ and $T_4(\xi)$ that are the most important terms of the equation in the damage zone; $T_2(\xi)$ and $T_3(\xi)$ are relatively insignificant. Thus, $T_1(\xi) \approx T_4(\xi)$ is a reasonable approximation for Eq. (16) inside the damage zone, which changes the response of the discontinuity function in that region. This response was termed "mass-affected", since the stiffness effects of $T_1(\xi)$ are now influenced by the inertial effects of $T_4(\xi)$. Finally, Fig. 18(b) shows the results of the intermediate case $\lambda_d = 0.06$, in which we observe nontrivial contributions from all terms except $T_2(\xi)$. The relevant approximation of Eq. (16) in the damage zone for this case is $T_1(\xi) \approx T_3(\xi) + T_4(\xi)$, since only the inertial term $T_2(\xi)$ can be deemed insignificant. Because both inertial and stiffness effects from the right-hand side of Eq. (16) come into play, we describe the response as "balanced". Note that the overall scale of the Eq. (16) terms in the balanced and mass-modified regimes is comparable to that of the damage scale, consistent with a much lower overall response from the discontinuity functions for these cases.

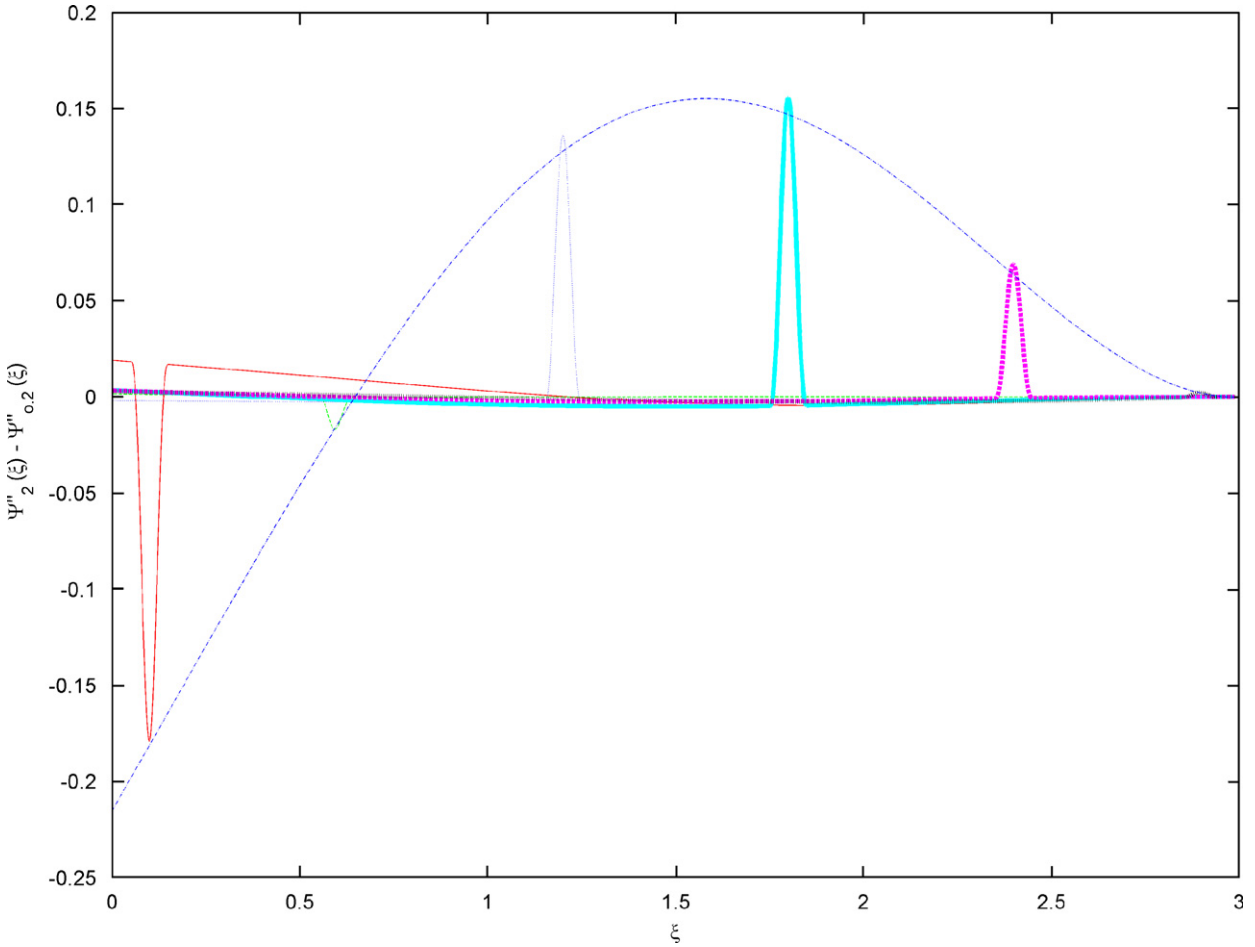

Fig. 17. Difference between nondimensional damaged and undamaged second mode curvatures due to changes in damage location compared to a scaled version of the undamaged second mode curvature. —— $\xi_d = 0.10$, — — — $\xi_d = 0.60$, · · · $\xi_d = 1.20$, ——— $\xi_d = 1.80$, — — — $\xi_d = 2.40$, ▪ ▪ ▪ $\xi_d = 2.90$, — · — $k\Psi''_{o,2}$.

There are two other general comments to be made regarding the magnitudes of the Eq. (16) terms. First, it can be shown that, outside of the damage zone, the term $T_3(\xi)$ is identically zero and thus plays no role in determining the behavior of the discontinuity function there. No general trends were observed among the remaining three terms outside of the damage zone, as they were usually all of the same approximate scale. Thus, there is no distinct characterization of the discontinuity function outside of the damage zone. Second, it should be mentioned that the mass-affected and balanced responses were relatively rare occurrences. The vast majority of responses studied can be classified as stiffness-dominated, especially when the assumption of top and bottom through-thickness cracks was made. The possibility of generating balanced or mass-modified responses depends crucially upon the parameter regime being studied; this issue will be explored more deeply in Section 4.

3.3. Continuous beam problem

3.3.1. General information

The final problem to be considered is that of a beam continuous across an intermediate support. This problem is chosen because it more closely emulates the geometry of actual bridges as compared to the previous problems studied. In the same spirit, we will employ a more realistic flexural rigidity model, namely the model for symmetric open cracks proposed by Christides and Barr [24] and shown in Eq. (4). (The use of enhanced

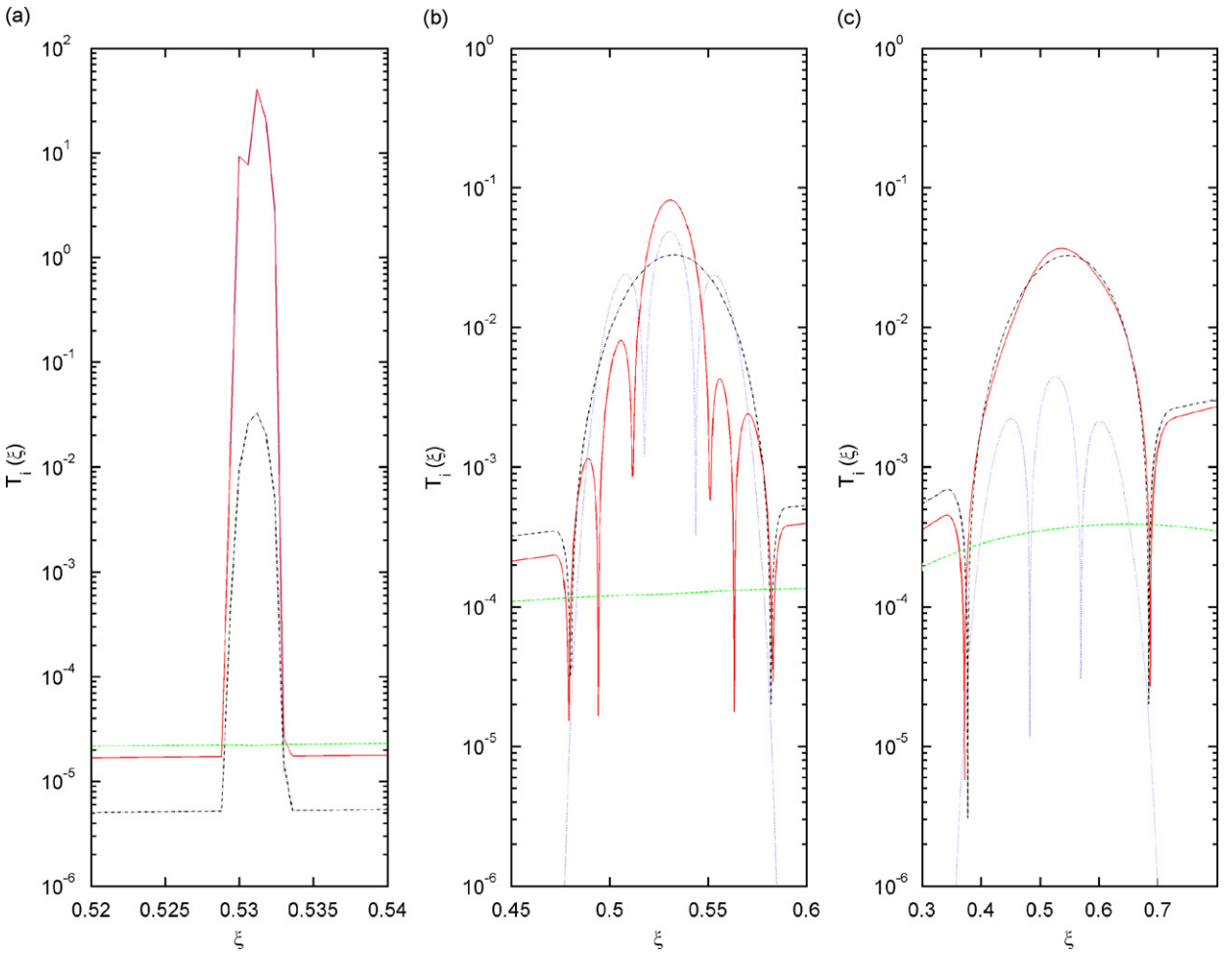

Fig. 18. Magnitudes of the four terms of Eq. (16) for a beam with mid-section cracks and various nondimensional damage radii. —— $T_1(\xi)$, — — — $T_2(\xi)$, · · · $T_3(\xi)$, — · — $T_4(\xi)$. (a) $\lambda_d = 0.002$, (b) $\lambda_d = 0.06$, (c) $\lambda_d = 0.2$.

versions of the Christides–Barr model—e.g., the model used in Ref. [27] —will be the subject of future work.) The relevant details of the problem we are considering are shown in Fig. 19. For simplicity, we assume a two-span beam with equal spans of length 1200 units. Note that the Christides–Barr stiffness model requires knowledge of the depth of the beam; a total depth of 36 units is assumed.

Turning our attention to the stiffness modification function, there are three parameters that must be specified in the function shown in Eq. (4). The stress profile parameter α was studied by Shen and Pierre [25], who obtained the value $\alpha = 1.936$ using a Galerkin procedure; this is the value used in our investigation. Next, the parameter d represents the half-depth of the beam, and thus $d = 18$ units in our problem. Finally, the parameter m can be shown to be the ratio of the undamaged cross section's moment of inertia over the moment of inertia for the cracked section. Thus, we should have $m > 1$ always but $m \approx 1$ for small levels of damage. Observing that the maximum reduction in stiffness occurs at $x = x_d$, we find that m is related to the parameter κ by $m = (1-\kappa)^{-1}$.

As was indicated in Section 2.1, a practical damage zone size can be established for the Christides–Barr model by setting a threshold below which the reduction in flexural rigidity from the undamaged value can be considered to be negligible; we define our damage zone according to the criterion

$$\frac{|EI(x) - EI_o|}{EI_o} < \varepsilon, \tag{17}$$

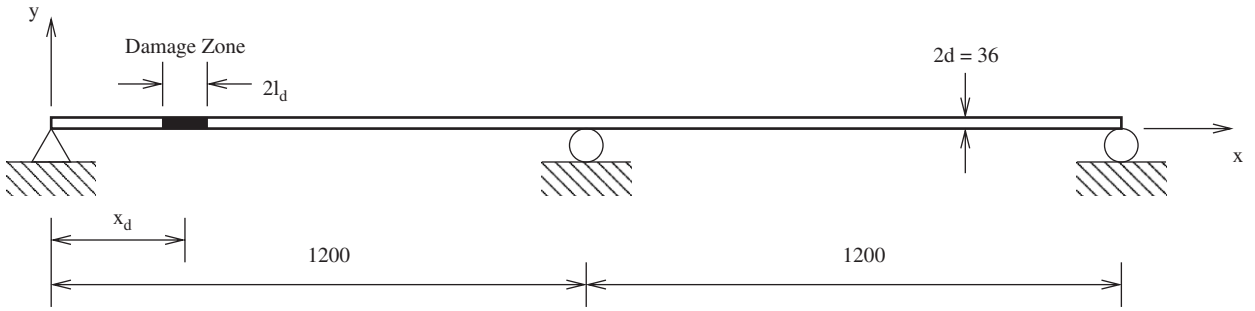

Fig. 19. The continuous beam problem.

where $\varepsilon \ll 1$ is a small parameter. Using this result and the previously discussed parameters, we find that the damage zone radius is related to κ and ε by

$$l_d = \frac{d}{2\alpha}\left\{\ln\left(\frac{1-\varepsilon}{\varepsilon}\right) + \ln\left(\frac{\kappa}{1-\kappa}\right)\right\} \tag{18}$$

and therefore the stiffness modification function can be represented as

$$\kappa\Delta(\eta) = 1 - \left\{1 + \frac{\kappa/(1-\kappa)}{\exp(\{\ln((1-\varepsilon)/\varepsilon) + \ln(\kappa/(1-\kappa))\}|\eta|)}\right\}^{-1}. \tag{19}$$

It can be shown that, for a fixed value of κ, each order of magnitude decrease in the size of ε gives an increase in the damage zone radius of approximately 10.7 units. For our problem, this means that decreasing ε by one order of magnitude causes the size of λ_d to increase by roughly 3.5% for Mode 1, with greater increases for the higher modes. Hence, using stricter tolerances in Eq. (17) can cause λ_d to become relatively large compared to the other parameters. Numerical tests revealed that there is a limiting value of ε such that any further lowering of the threshold produces negligible changes in output. In our work, ε is always chosen such that this limit has been reached.

We note that this stiffness model does not account for mass loss, so we will need to impose our own mass modification model. We chose to mimic the behavior of the simplified damage model, in which it can be shown that $\Gamma(\eta)$ and $\Delta(\eta)$ are essentially the same function for low levels of damage. Thus, we employ Eq. (19) to describe the mass modification function $\Gamma(\eta)$, replacing $\Delta(\eta)$ with $\Gamma(\eta)$ and κ with μ. It can be shown that the percent reduction in area corresponding to a given value of m scales as m^{-3} for through-thickness cracks, and thus we expect the maximum loss of mass (assumed to be proportional to area) to scale as $1-m^{-3}$. Thus, we take the parameter μ to be given by $\mu = 1 - \sqrt[3]{1-\kappa}$ using the previously found relationship between m and κ.

The mode shapes of the undamaged beam fall into two categories, distinguished by their symmetry with respect to the center support. The odd-numbered modes are anti-symmetric with respect to the center and have the form

$$\Psi_{o,2n-1}(\xi) = \sin\left(\frac{\pi\xi}{2}\right), \tag{20}$$

with a corresponding nondimensional beam length $\Lambda_{2n-1} = 4n$. These modes are identical to the even-numbered modes from the simply supported beam problem (see Eq. (11)). As for the even-numbered modes of this problem, they are symmetric with respect to the center and can be written as

$$\Psi_{o,2n}(\xi) = \begin{cases} A_{2n}\left[\sin\left(\frac{\pi}{2}\xi\right) - \left\{\dfrac{\sin\left(\frac{\pi}{4}\Lambda_{2n}\right)}{\sinh\left(\frac{\pi}{4}\Lambda_{2n}\right)}\right\}\sinh\left(\frac{\pi}{2}\xi\right)\right], & 0 \leqslant \xi \leqslant \frac{1}{2}\Lambda_{2n} \\ A_{2n}\left[\sin\left(\frac{\pi}{2}(\Lambda_{2n}-\xi)\right) - \left\{\dfrac{\sin\left(\frac{\pi}{4}\Lambda_{2n}\right)}{\sinh\left(\frac{\pi}{4}\Lambda_{2n}\right)}\right\}\sinh\left(\frac{\pi}{2}(\Lambda_{2n}-\xi)\right)\right], & \frac{1}{2}\Lambda_{2n} \leqslant \xi \leqslant \Lambda_{2n} \end{cases} \tag{21}$$

where the nondimensional beam length Λ_{2n} satisfies the relation $\tan((\pi/4)\Lambda_{2n}) = \tanh((\pi/4)\Lambda_{2n})$. For sufficiently large values of Λ_{2n}, it can be shown that $\Lambda_{2n} \approx 4n+1$. See Ref. [30] for details. The normalization parameter $A_{2n} = 0.93508$, with the maximum modal displacement always occurring at the peaks just before and after the central support.

3.3.2. Effectiveness of higher order derivatives as damage indicators

To illustrate the effectiveness of higher order derivatives as damage indicators, we simulated the damage location process by examining the changes induced in mode shapes, modal curvatures, and modal fourth derivatives at discrete locations in the beam for varying levels of stiffness loss. In particular, we examined Mode 2 vibration of the continuous beam ($\Lambda_2 = 4.9995$) and a fixed location for the damage ($\chi_d = 1.75$). We employed Eq. (19) as our stiffness loss model for four values of stiffness loss: $\kappa = 0.30$, 0.10, 0.03, and 0.01. (Note that the nondimensional damage zone radius varied only from 0.10330 to 0.066998 as κ decreased; this reflects the dependence of l_d on ε, which was set at $\varepsilon = 10^{-5}$.) We chose to measure the response at eleven locations along the first span of the continuous beam, with the spacing between measurement locations taken to be 108 units. With this choice of spacing, it can be shown that the eighth sensor is located closest to the damage, at $\xi = 1.80$. This reflects the most common measurement situation, in which a sensor (for a sufficiently refined grid) is close to but not on top of a damage location.

The results of this study are shown in Figs. 20–22. (For simplicity, only the left span of the beam—the one containing the damage—is shown.) In these figures we plot the percent change in the various modal quantities from their expected "undamaged" values for the previously selected stiffness loss levels. In Fig. 20, we indicate the percent change in the actual mode shape due to the four damage levels. As one would expect, decreasing the value of κ caused an overall decrease in the magnitude of the percentage changes, with virtually no change observed for the lowest stiffness loss level. Even for the most severe damage case ($\kappa = 0.30$), the percent changes in mode shape are relatively low; in fact, they are always lower in magnitude than the corresponding stiffness loss value. Moreover, the damage location cannot be accurately determined from these changes, as maximum changes tended to occur near the central support. (This is somewhat an artifact of the "small divisors" problem, since the mode shape values themselves are fairly small as one approaches the central support.) Once again, we are led to the conclusion, consistent with that found by other researchers, that mode shape changes are only fair indicators of the presence of damage and are not good indicators of damage location.

When one examines the percent changes in modal curvature (Fig. 21), this situation improves noticeably. For the larger values of stiffness loss studied here ($\kappa = 0.30$ and 0.10), one finds very large percent changes in the modal curvature at the sensor closest to the damage location—a very strong indicator of both the location and severity of the damage. However, the induced changes in curvature are less distinct when the smaller stiffness loss parameters ($\kappa = 0.03$ and 0.01) are considered, making the location of the damage less obvious. Still, the modal curvature values in general seem to provide a good indication of damage location and severity, although its sensitivity to low levels of damage may not be strong.

Similar features are noted upon considering the percent changes in modal fourth derivative (Fig. 22). We first note that the higher levels of stiffness loss are associated with large indications of percent change, although not as large as those observed in the modal curvatures. When the lower stiffness loss levels were considered, we found smaller but significant deviations in the modal fourth derivative values. In all cases, the damage location is distinctly indicated by the change in modal fourth derivative. Thus, both the modal curvatures and modal fourth derivatives appear to be strong damage indicators for relatively high levels of damage, and the modal fourth derivatives appear to perform reasonably well at relatively small damage levels.

4. Approximations for higher order derivative discontinuities

4.1. General considerations

Having studied the influence of damage on the mode shape properties numerically, we now wish to obtain some analytical approximations of the higher derivatives of the discontinuity function $\Phi_n(\xi)$ via a formal analysis. This entails finding approximate relations in Eq. (16) that can simplify this equation and thus permit

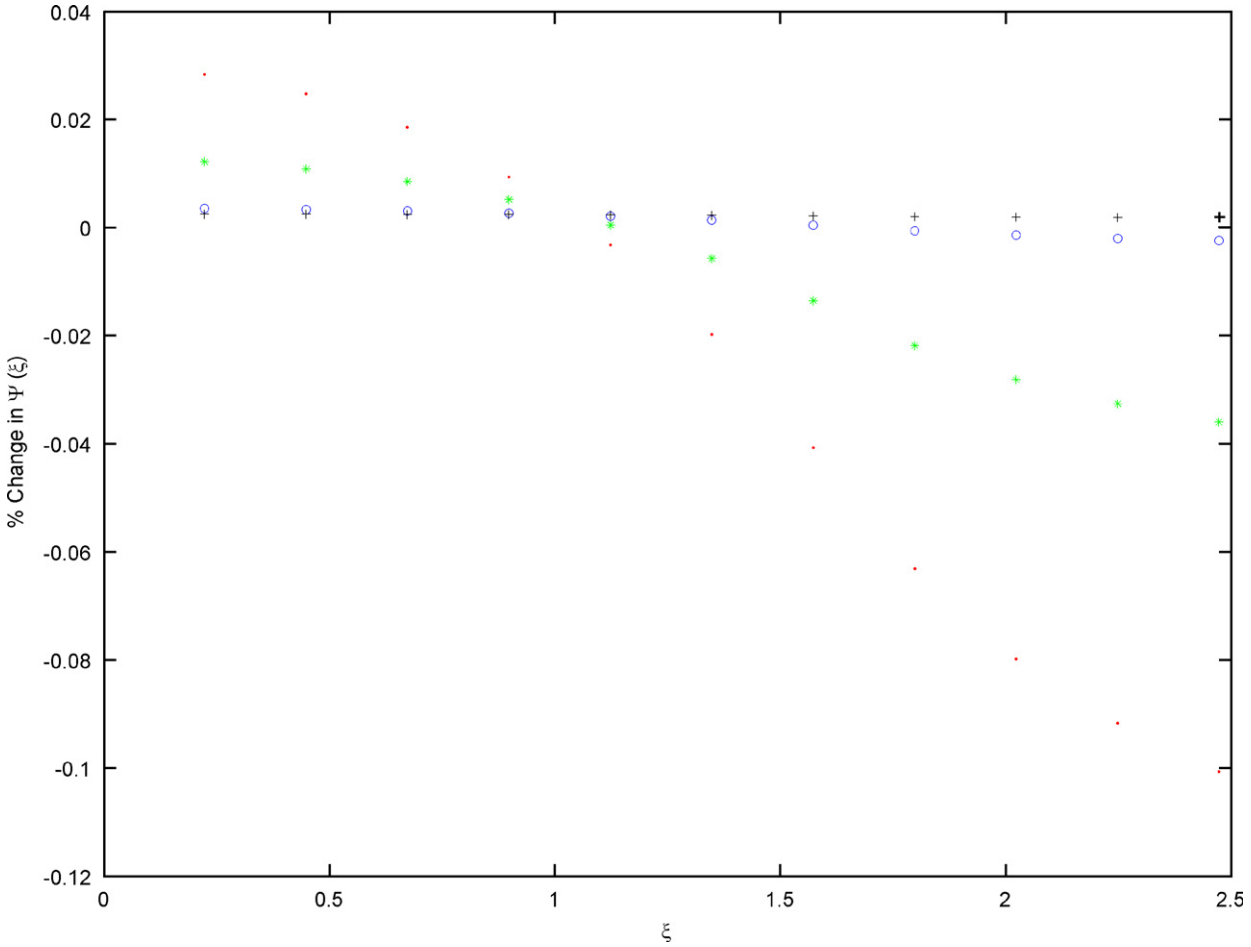

Fig. 20. Percent change in mode shape values at selected locations for various κ values. · $\kappa = 0.30$, * $\kappa = 0.10$, ○ $\kappa = 0.03$, + $\kappa = 0.01$.

formal solutions to be found. To pursue this, we introduce the small value $\varepsilon \ll 1$ and scale the damage parameters as follows:

$$\lambda_d = \bar{\lambda}_d \varepsilon^{\ell}, \quad \kappa = \bar{\kappa} \varepsilon^{k}, \quad \mu = \bar{\mu} \varepsilon^{m}. \tag{22}$$

(The exponent k is not related to the exponent in the loss of depth function shown in Eq. (14).) All barred quantities are assumed to be $\mathcal{O}(\varepsilon^0)$, and k and m are required to be nonnegative. This requirement stems from the fact that κ and μ represent percent changes in physical quantities that cannot exceed 100%. Notice that $\mathcal{O}(\kappa) = \mathcal{O}(\varepsilon^0)$ or $\mathcal{O}(\mu) = \mathcal{O}(\varepsilon^0)$ essentially implies that a substantial majority of the cross section has been lost and thus that the structure is in a state of impending collapse; such situations are extreme cases that are not expected to be encountered in general structural health monitoring applications. Therefore, $k > 0$ and $m > 0$ are reasonable assumptions on the loss coefficients. Notice also that the exponent l could legitimately take on either positive or negative values—the latter case corresponds to the situation in which the extent of the damage is comparable to or significantly larger than the modal length scale $L_{o,n}$. This is most likely to occur when the damage is due to the action of a global damaging mechanism or when the mode under consideration has a very high frequency and thus a correspondingly short wavelength. For simplicity of our analysis, we do not consider this possibility and therefore assume that $l > 0$. Finally, we note that $\pi^4/16$ represents an $\mathcal{O}(\varepsilon^0)$ quantity; this becomes obvious as $\varepsilon \to 0$.

Before commencing with the analysis, we make three observations. First, the rescaling of $Y_{o,n}(x)$ to $\Psi_{o,n}(\xi)$ introduced via Eq. (8) guarantees that the normalization assumption on $Y_{o,n}(x)$ transfers directly to $\Psi_{o,n}(\xi)$. This result, along with the assumed properties of the functions $\Delta(\eta(\xi))$ and $\Gamma(\eta(\xi))$, shows that these three

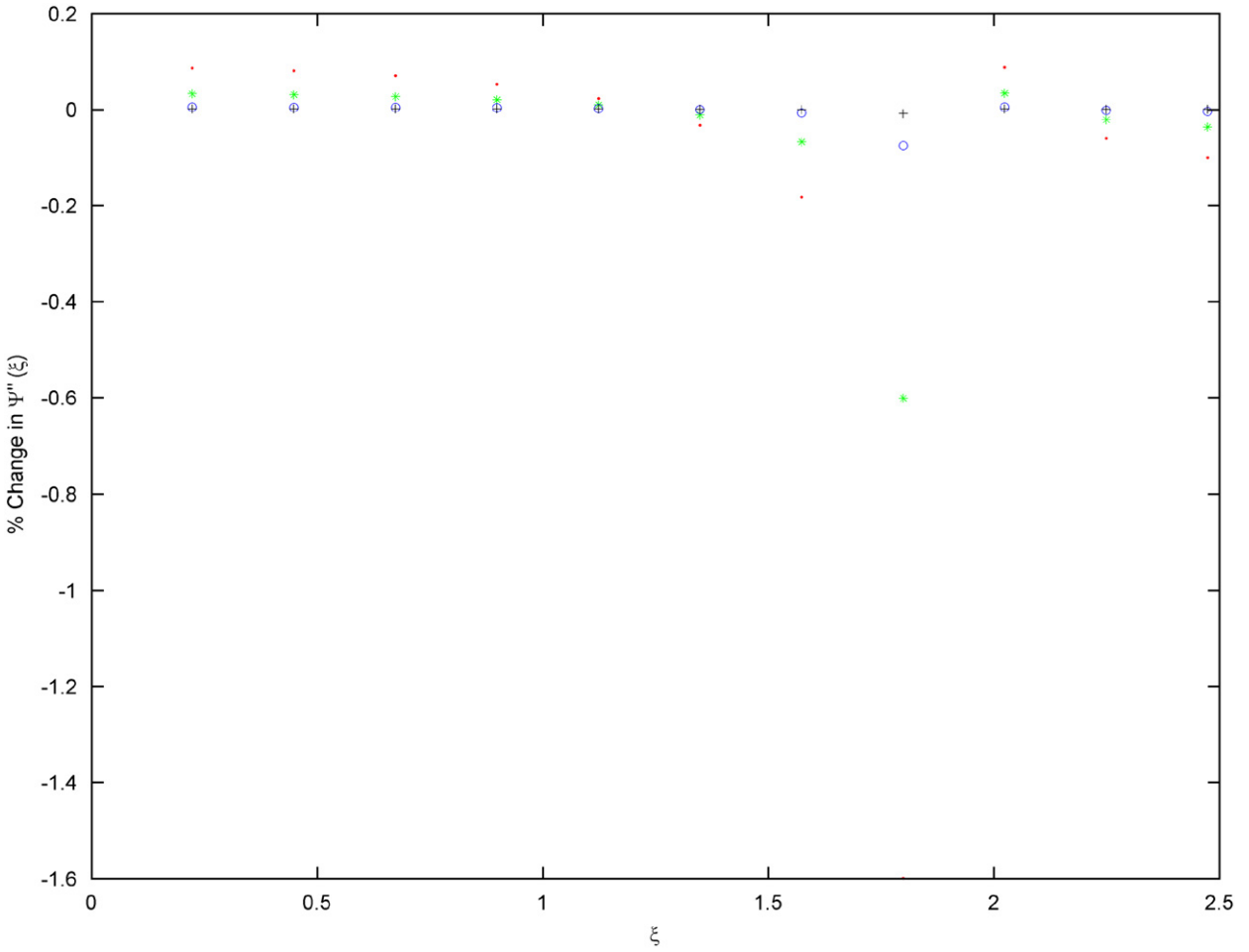

Fig. 21. Percent change in modal curvature values at selected locations for various κ values. · $\kappa = 0.30$, * $\kappa = 0.10$, ○ $\kappa = 0.03$, + $\kappa = 0.01$.

functions are finite-sized (i.e., $\mathcal{O}(\varepsilon^0)$) over most of the damage zone. In other words, while small values are possible, one typically expects these functions not to be small. Second, the rescaling of the mode shapes leads to the requirement that the jth derivative of $\Psi_{o,n}(\xi)$ be proportional to $(\pi/2)^j$. Thus, all derivatives of $\Psi_{o,n}(\xi)$ with respect to ξ are $\mathcal{O}(\varepsilon^0)$ quantities in general. (It may be argued that $(\pi/2)^j$ becomes large for a large enough value of j, which implies that the corresponding derivative is large. However, since the magnitude of the derivative is still bounded, $\mathcal{O}(\varepsilon^0)$ is still a reasonable estimate.) Third, the assumed properties of $\Delta(\eta)$ allow us to argue that both the first and second derivative of $\Delta(\eta)$ with respect to η must take on $\mathcal{O}(\varepsilon^0)$ values over at least part of the damage zone. The details of this argument are presented in Section A.1 of the Appendix A. Again, it is emphasized that neither the derivatives of $\Psi_{o,n}(\xi)$ with respect to ξ nor the derivatives of $\Delta(\eta)$ with respect to η are restricted from taking on small values; indeed, the derivatives of $\Delta(\eta)$ with respect to η are zero outside of the damage zone, so continuity requires that they stay small for at least some portion (however miniscule) of the damage zone near the edges. However, these observations permit us to make reasonably generic conclusions regarding the behavior of the derivatives of $\Phi_n(\xi)$, which is our main concern.

4.2. Formal analysis

4.2.1. Case 1: inside the damage zone—stiffness-dominated behavior

Recalling the discussion in Section 3.2.2, we anticipate that there are three distinct approximations that can be made on Eq. (16) to determine the behavior of $\Phi_n(\xi)$ in the damage zone. In this section, we investigate the

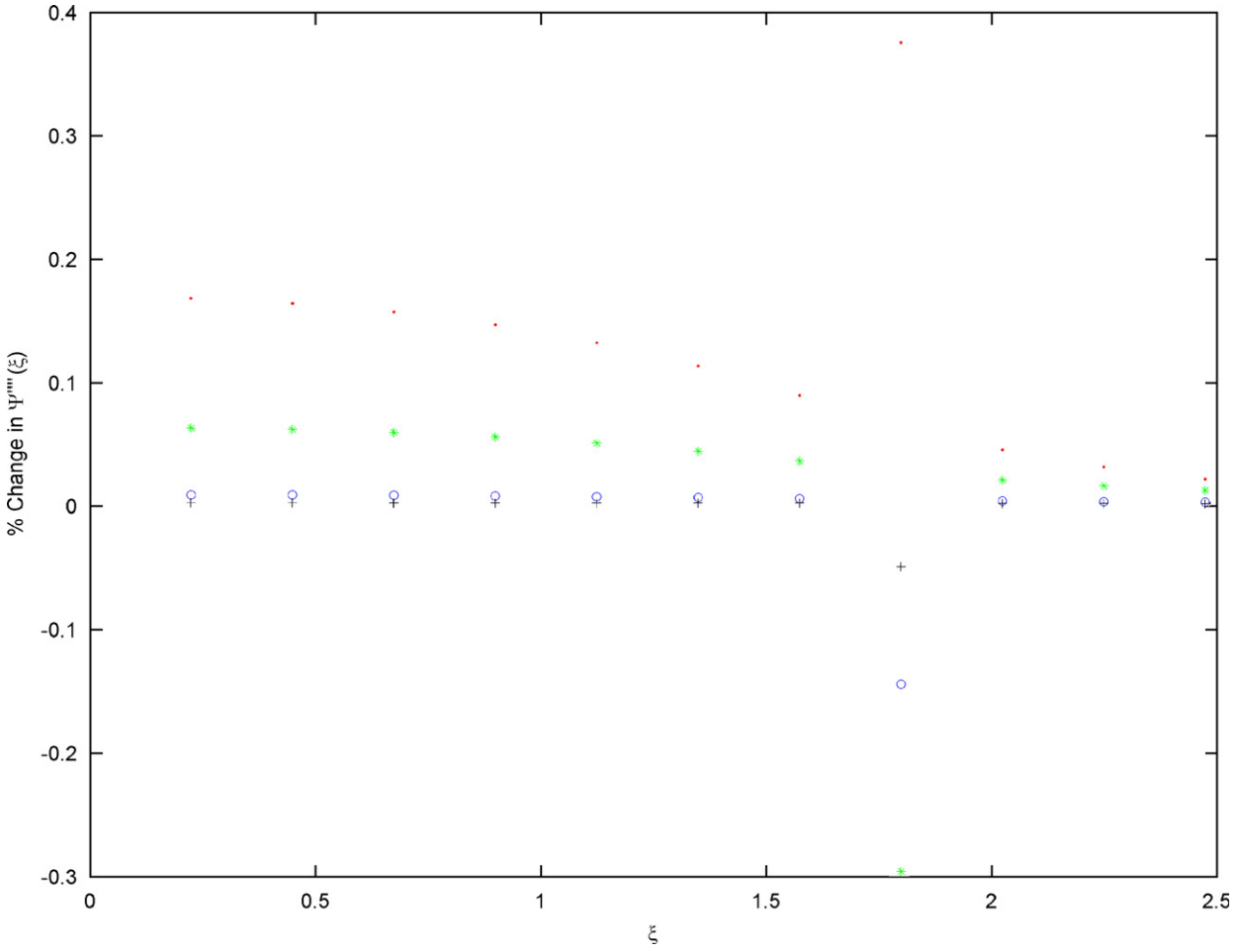

Fig. 22. Percent change in modal fourth derivative values at selected locations for various κ values. · $\kappa = 0.30$, * $\kappa = 0.10$, ○ $\kappa = 0.03$, + $\kappa = 0.01$.

most commonly observed situation, namely stiffness-dominated behavior. We assume that $k = m$, which requires that the stiffness loss and mass loss effects be comparable in magnitude. (This was typical of the stiffness-dominated cases studied; the case $k \neq m$ will be discussed in a later section.) Based on these assumptions, we draw a series of conclusions regarding the orders of terms in Eq. (16), starting with the right-hand side of this equation.

The term $T_3(\xi)$ represents the effects of changes in the underlying internal bending moments due to damage. We expand this to give:

$$T_3(\xi) = \frac{\mathrm{d}^2}{\mathrm{d}\xi^2}\left[\kappa \Delta(\eta(\xi)) \frac{\mathrm{d}^2 \Psi_{o,n}(\xi)}{\mathrm{d}\xi^2}\right] = \kappa \Delta(\eta) \Psi''''_{o,n}(\xi) + \frac{2\kappa}{\lambda_d} \Delta'(\eta) \Psi'''_{o,n}(\xi) + \frac{\kappa}{\lambda_d^2} \Delta''(\eta) \Psi''_{o,n}(\xi). \tag{23}$$

Once again, $\Delta(\eta(\xi))$ and $\Psi_{o,n}(\xi)$ and their derivatives are generically $\mathcal{O}(\varepsilon^0)$ within the damage zone, so the coefficients determine the order of this term. The orders of the coefficients are

$$\kappa = \mathcal{O}(\varepsilon^k), \quad \frac{2\kappa}{\lambda_d} = \mathcal{O}(\varepsilon^{k-\ell}), \quad \frac{\kappa}{\lambda_d^2} = \mathcal{O}(\varepsilon^{k-2\ell}). \tag{24}$$

We observe that the coefficient of the third term must have largest magnitude, since $\ell > 0$. Thus, for damage of limited extent, we expect that the behavior of $T_3(\xi)$ in the damage zone is governed by the third term and hence

the entire term is generally $\mathcal{O}(\varepsilon^{k-2\ell})$. Moreover, this term will be large in an absolute sense when $\ell \geqslant \frac{1}{2}k$. This condition speaks to the relative importance of damage extent in determining overall behaviors of the modal discontinuities.

There is one non-generic situation that deserves some consideration for its effect upon $T_3(\xi)$. As seen in Section 3.1.4, it is possible for $\Delta(\eta)$ to have abrupt variations that can lead to very large values for $\Delta'(\eta)$ and $\Delta''(\eta)$. Thus, it is possible for either of these derivatives to have magnitudes of $\mathcal{O}(\varepsilon^{-d})$ with $d>0$. (Note that it is not expected that both derivatives take on large values at the same location in the damage zone; if one derivative has a large magnitude, the other one is still likely to be an $\mathcal{O}(\varepsilon^0)$ term.) If $\Delta''(\eta)$ takes on $\mathcal{O}(\varepsilon^{-d})$ values at a certain location in the damage zone, then the overall estimate of the magnitude of the third term becomes $\mathcal{O}(\varepsilon^{k-2\ell-d})$, an increase in the overall size of $T_3(\xi)$. If, however, $\Delta'(\eta)$ takes on $\mathcal{O}(\varepsilon^{-d})$ values, then the estimated size of the second term is $\mathcal{O}(\varepsilon^{k-\ell-d})$, which could be equal to or even greater than the estimated size of the third term, $\mathcal{O}(\varepsilon^{k-2\ell})$. This would lead us to conclude that the second term could not be neglected in any estimate of $T_3(\xi)$. Thus, it may not always be a good idea to approximate $T_3(\xi)$ by the third term in Eq. (23), as one could be underestimating the effect of $T_3(\xi)$ on Eq. (16) by doing so.

Next we turn our attention to $T_4(\xi)$, which represents changes in the initial inertial force associated with direct mass loss and with shifting of the frequency of vibration. Since $\Gamma(\eta(\xi))$ and $\Psi_{o,k}(\xi)$ are expected to be $\mathcal{O}(\varepsilon^0)$ over most of the damage zone, the orders of the mass loss coefficient μ and frequency shift Ω_n^2-1 govern this term's order in this region. We note that the exact value of Ω_n^2 cannot be determined without solving the full problem posed by Eq. (10). However, a simple argument presented in Section A.2 of the Appendix A shows that $\Omega_n^2 \approx 1$ but that the size of Ω_n^2-1 is $\mathcal{O}(\varepsilon^{m+\ell})$. Based on this, it is expected that the overall size of $T_4(\xi)$ is $\mathcal{O}(\varepsilon^m)$ and thus is not comparable to the $\mathcal{O}(\varepsilon^{k-2\ell})$ terms associated with $T_3(\xi)$. Hence, $T_3(\xi)$ dominates $T_4(\xi)$ asymptotically, justifying our ignoring of these inertial effects when estimating the overall order of the right-hand side of Eq. (16).

It is more difficult to make generalizations concerning the left-hand side of Eq. (16), since the sizes of $\Phi_n(\xi)$ and its derivatives are obviously undetermined. However, our numerical evidence from Section 3.2.2 clearly indicates that one expects $T_1(\xi) \gg T_2(\xi)$ inside of the damage zone whenever stiffness-dominated behavior prevails. One can also argue that the inertial term $T_2(\xi)$ should not be expected to make a significant contribution to this portion of the equation. To see this, we note that assuming this inertial term to be significant implies that $\mathcal{O}((\pi^4/16)\Omega_n^2\{1-\mu\Gamma(\eta(\xi))\}\Phi_n(\xi)) = \mathcal{O}(\varepsilon^{k-2\ell})$ or lower. Since all of the other factors in this expression are generically $\mathcal{O}(\varepsilon^0)$ or higher in the damage zone, this assumption requires that $\mathcal{O}(\Phi_n(\xi)) = \mathcal{O}(\varepsilon^{k-2\ell})$; i.e., the change in the mode shape should be large whenever $\ell \geqslant \frac{1}{2}k$. We point out, however, that no researchers in the literature have claimed to find large changes in the mode shape induced by damage, even for damage of reasonably large magnitude ($k=0$). Based on this observation, we consider it unlikely (but not impossible) that $T_2(\xi)$ contributes significantly to the overall behavior of Eq. (16).

Based upon these results and assumptions, we are led to the following approximate relationship for Eq. (16) whenever stiffness-dominated behavior applies:

$$\frac{\mathrm{d}^2}{\mathrm{d}\xi^2}\left[\{1-\kappa\Delta(\eta(\xi))\}\frac{\mathrm{d}^2\Phi_n(\xi)}{\mathrm{d}\xi^2}\right] \approx \frac{\mathrm{d}^2}{\mathrm{d}\xi^2}\left[\kappa\Delta(\eta(\xi))\frac{\mathrm{d}^2\Psi_{o,n}(\xi)}{\mathrm{d}\xi^2}\right]. \tag{25}$$

By formally integrating Eq. (25) twice and performing some algebra, we obtain

$$\Phi_n''(\xi) \approx \frac{\kappa\Delta(\eta(\xi))}{1-\kappa\Delta(\eta(\xi))}\Psi_{o,n}''(\xi) + \frac{A+B(\xi-\xi_d)}{1-\kappa\Delta(\eta(\xi))}, \tag{26}$$

where A and B are constants of integration. Assuming continuity of $\Phi_k''(\xi)$ leads to the following:

$$A = \frac{\Phi_n''(\xi_d+\lambda_d)+\Phi_n''(\xi_d-\lambda_d)}{2}, \quad B = \frac{\Phi_n''(\xi_d+\lambda_d)-\Phi_n''(\xi_d-\lambda_d)}{2\lambda_d}. \tag{27}$$

The approximation obtained can be considered to be a combination of local effects of the damage expressed by the stiffness modification term and global effects of the damage (i.e., effects arising from outside of the damage zone) expressed by the constants of integration. This result was the motivation for the use of $\kappa\Psi_{o,n}''(\xi)$ in Fig. 18; Eq. (26) implies that $\Phi_n''(\xi_d) \approx (\kappa\Psi_{o,n}''(\xi_d)+A)/(1-\kappa)$ and so $\kappa\Psi_{o,n}''(\xi_d)$ gives a somewhat rougher estimate of the expected change in the modal curvature at the center of the damage zone.

Although we do not have general estimates of the magnitude of the integration constants, we point out that we typically expect that the magnitude of B exceeds that of A due to the factor of λ_d in the denominator of B. This statement, however, assumes that $\mathcal{O}(\Phi_n''(\xi_d+\lambda_d)+\Phi_n''(\xi_d-\lambda_d))$ is equal to $\mathcal{O}(\Phi_n''(\xi_d+\lambda_d)-\Phi_n''(\xi_d-\lambda_d))$, which may not be true if $\Phi_n''(\xi_d-\lambda_d)$ and $\Phi_n''(\xi_d+\lambda_d)$ are sufficiently close in value. Numerical evidence suggests that it is possible to have A larger in magnitude than B, so we do not want to discount this possibility in our subsequent analyses. It can also be stated that the second term on the right-hand side of Eq. (26) makes a significant contribution to the approximation for $\Phi_n''(\xi)$ only if $\mathcal{O}(A)=\mathcal{O}(\varepsilon^k)$ or lower and/or if $\mathcal{O}(B)=\mathcal{O}(\varepsilon^{k-\ell})$ or lower.

We can obtain further approximations on the higher derivatives of $\Phi_n(\xi)$ from Eq. (26). Taking a derivative with respect to ξ and simplifying algebraically, we obtain

$$\Phi_n'''(\xi)\approx\frac{\kappa}{\lambda_d}\frac{\Delta'(\eta)}{\{1-\kappa\Delta(\eta)\}^2}\Phi_{o,n}''(\xi)+\frac{\kappa\Delta(\eta)}{1-\kappa\Delta(\eta)}\Psi_{o,n}'''(\xi)+\frac{B}{1-\kappa\Delta(\eta)}+\frac{\kappa}{\lambda_d}\frac{\Delta'(\eta)(A+B(\xi-\xi_d))}{\{1-\kappa\Delta(\eta)\}^2}. \tag{28}$$

Once again, all of the functions appearing in this result are estimated to be $\mathcal{O}(\varepsilon^0)$ in the damage zone, so the coefficients determine the overall behavior. Eq. (24) tells us that the second term in Eq. (28) is expected to make little contribution to the overall magnitude of $\Psi_n'''(\xi)$, since this term should be of higher order in ε compared to the first term for $\ell>0$. As for the third and fourth terms of Eq. (28), we reiterate that we do not have any formal estimates of the size of the integration constants, so generic claims regarding these two terms are difficult to make. One way to gain some insight into the importance of these two terms is to assume that $\mathcal{O}(A)=\mathcal{O}(\varepsilon^k)$ and $\mathcal{O}(B)=\mathcal{O}(\varepsilon^{k-\ell})$, so that the second term on the right-hand side of Eq. (26) does make a significant contribution to $\Phi_n''(\xi)$. It can then be shown that the fourth term in Eq. (28) has a generic size of $\mathcal{O}(\varepsilon^{2k-\ell})$ and thus would be less significant than the third term so long as the stiffness loss level is not $\mathcal{O}(\varepsilon^0)$. Under such circumstances, we can approximate $\Phi_n'''(\xi)$ as follows:

$$\Phi_n'''(\xi)\approx\frac{\kappa}{\lambda_d}\frac{\Delta'(\eta)}{\{1-\kappa\Delta(\eta)\}^2}\Psi_{o,n}''(\xi)+\frac{B}{1-\kappa\Delta(\eta)}. \tag{29}$$

Of course, the actual behaviors of A and B, as well as any possible large contributions from $\Delta'(\eta)$, could render this result invalid. However, under this hypothesis, we observe that the factor κ/λ_d determines the overall size of the third derivative changes and that potentially large changes can be expected even for small levels of damage if the spatial scale of the damage is appropriately small. Thus, changes in the third derivative are potentially much larger than the curvature changes (which have an overall size estimate of $\mathcal{O}(\varepsilon^k)$), making such changes easier to find. From this, we infer that the damage radius scale λ_d plays an important role in determining robustness of a higher order derivative as a damage indicator.

We follow a similar process to obtain approximations for the fourth derivative of the discontinuity function. Based on our experience with the previous calculation, we recognize that the most significant contributions to $\Phi_n''''(\xi)$ will come from terms resulting from derivatives of the stiffness modification function $\Delta(\eta(\xi))$ with respect to ξ, as such terms will generate factors of λ_d^{-1} that will magnify their size. Conversely, terms resulting from a derivative of the undamaged curvature $\Psi_{o,k}''(\xi)$ will not contribute significantly, since such derivatives are still expected to be $\mathcal{O}(\varepsilon^0)$. Once again, predicting the importance of the terms involving integration constants is a difficult task, but a reasonable argument can be made that such terms should not make significant contributions to $\Phi_n''''(\xi)$ due to their overall small size. Taking these factors into account, we arrive at the following result:

$$\Phi_n''''(\xi)\approx\frac{\kappa}{\lambda_d^2}\frac{1}{\{1-\kappa\Delta(\eta)\}^2}\left[\Delta''(\eta)+\frac{2\kappa(\Delta'(\eta))^2}{1-\kappa\Delta(\eta)}\right]\Psi_{o,n}''(\xi). \tag{30}$$

This derivative will be large in an absolute sense whenever $k\leqslant 2\ell$, which is a relatively unrestrictive requirement. Thus, even small levels of damage have the potential to generate large changes in the mode shape fourth derivative, making this derivative a prime candidate for the robust damage indicator discussed in Section 1.

A comparison of these approximations with the corresponding numerical results is provided in Fig. 23. We consider the simply supported beam problem, Mode 1 vibration, and the simplified damage model with

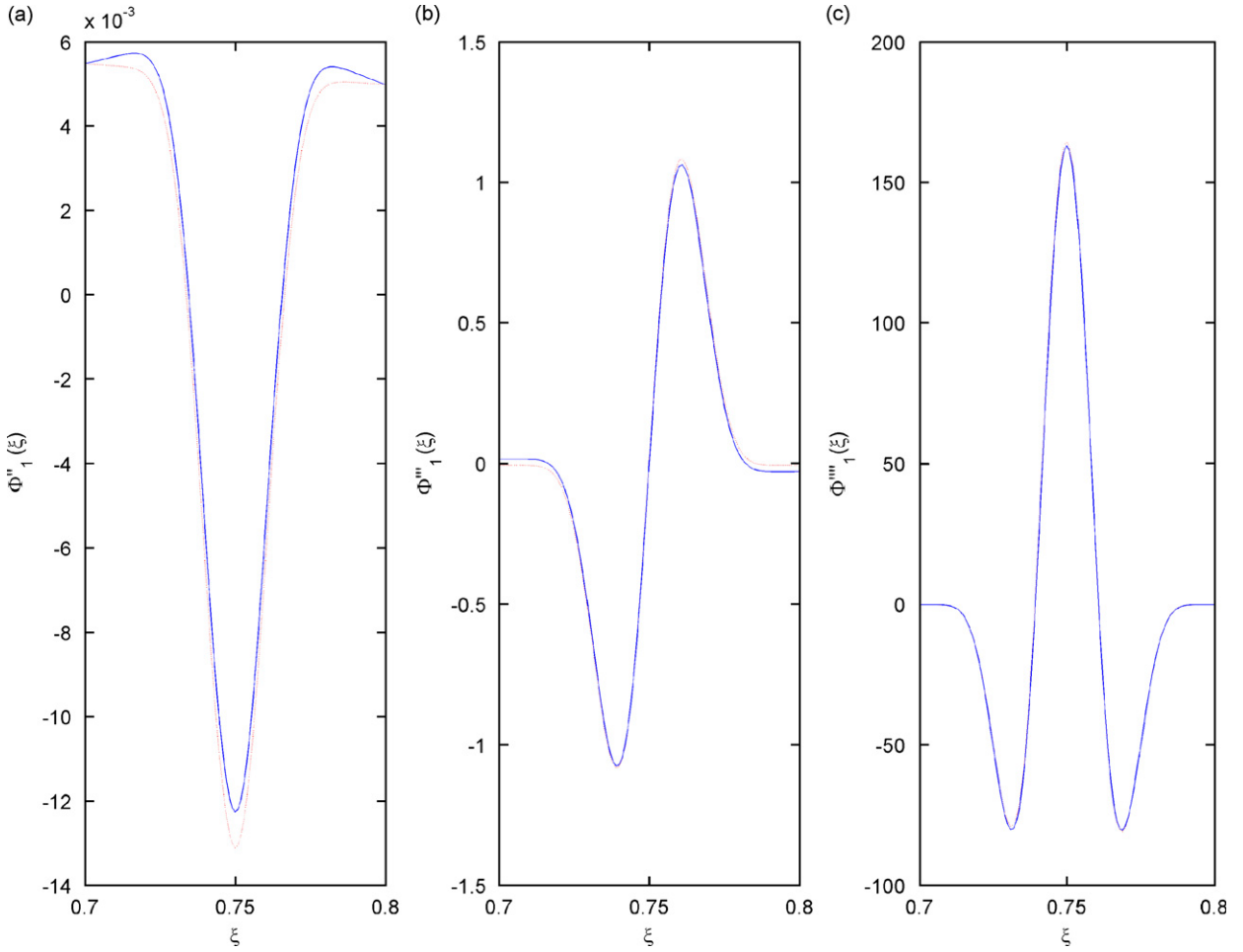

Fig. 23. Comparison of analytical approximations and numerical results for the simply-supported beam problem with stiffness-dominated behavior. —— numerical result, · · · analytical approximation. (a) $\Phi_1''(\xi)$, (b) $\Phi'''_1(\xi)$, (c) $\Phi''''_1(\xi)$.

mid-section cracks and $k = 1$. We set the damage level to be $\delta = 0.2$; thus, $\mu = 0.2$ and $\kappa = 0.008$. Finally, we take $\xi_d = 0.75$ and $\lambda_d = 0.05$; note that these choices of parameters are expected to lead to stiffness-dominated behavior, since $\kappa/\lambda_d^2 = 3.2 \gg \mu = 0.2$. As seen in Fig. 24, the approximate analytical results from Eqs. (26), (29), and (30) compare very well to the "exact" numerical integrations of the damage-induced discontinuities in the damage zone. The approximations even appear to become more accurate as the order of the derivative discontinuity increases, although scaling plays a role in this. Nevertheless, we feel that the analytical approximations give a good estimation of the expected behavior in the damage zone, justifying their use in diagnosing higher order derivative discontinuity behavior.

4.2.2. Case 2: inside the damage zone—mass-affected behavior

The assumption of mass-affected behavior leads to a different approach to the problem of finding approximations for the higher order modal derivatives. As discussed above, the term $T_4(\xi)$ now dominates $T_3(\xi)$, leading to the following approximate version of Eq. (16):

$$\frac{d^2}{d\xi^2}\left[\{1-\kappa\Delta(\eta(\xi))\}\frac{d^2\Phi_n(\xi)}{d\xi^2}\right] \approx \left(\frac{\pi}{2}\right)^4\left[\Omega_n^2 - 1 - \mu\Omega_n^2\Gamma(\eta(\xi))\right]\Psi_{o,n}(\xi). \tag{31}$$

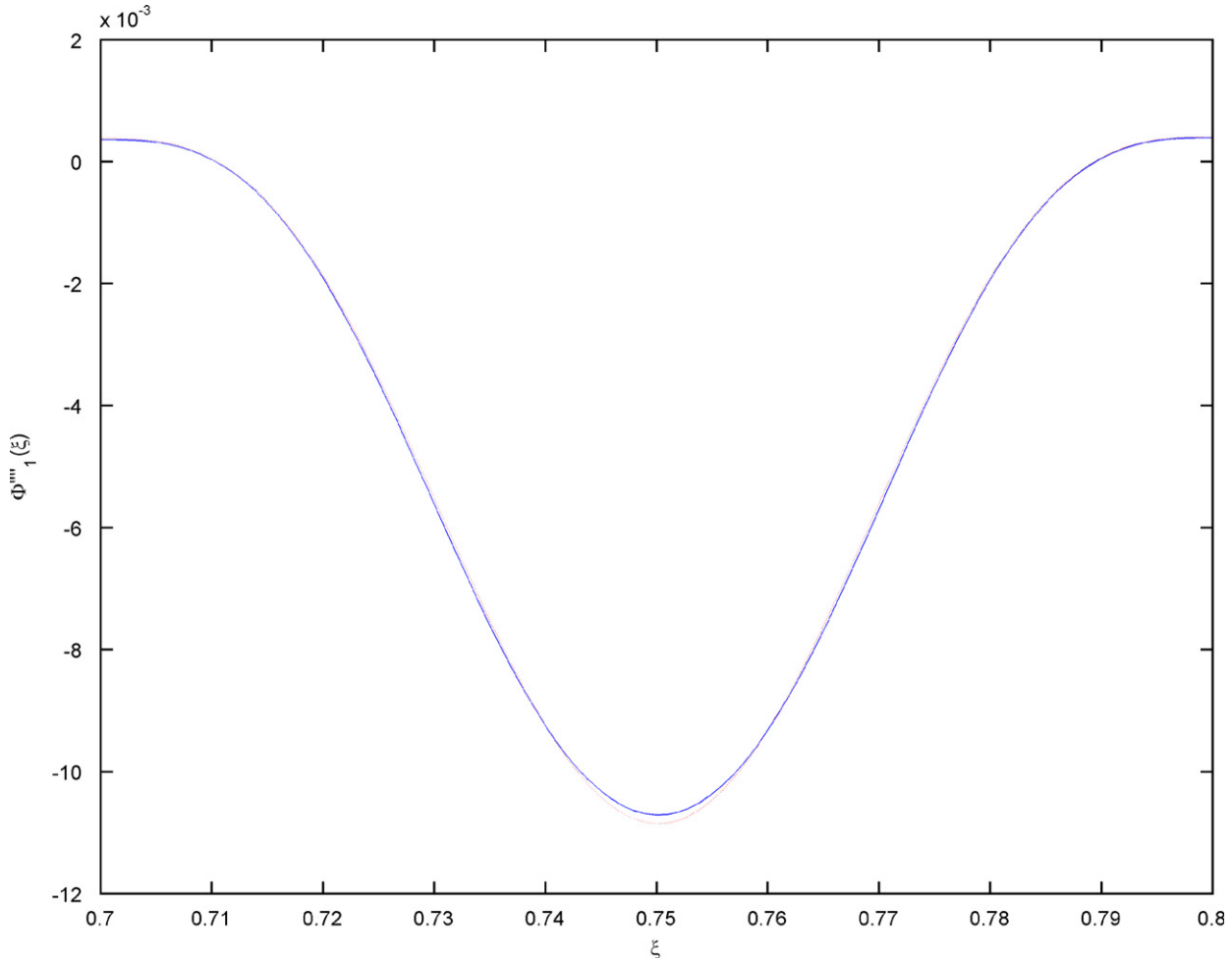

Fig. 24. Comparison of analytical approximations and numerical results for $\Phi''''(\xi)$ in the simply-supported beam problem with mass-affected behavior. —— numerical result, · · · analytical approximation.

We formally integrate this equation on both sides twice from the left edge of the damage zone to an arbitrary location in the interior of the damage zone:

$$\Phi_n''(\xi) \approx \frac{(\pi/2)^4}{1-\kappa\Delta(\eta(\xi))} \int_{\xi_d-\lambda_d}^{\xi} \int_{\xi_d-\lambda_d}^{\xi'} \left[\Omega_n^2 - 1 - \mu\Omega_n^2 \Gamma(\eta(\xi''))\right] \Psi_{o,n}(\xi'')\mathrm{d}\xi''\mathrm{d}\xi' + \frac{\bar{A} + \bar{B}(\xi - \xi_d + \lambda_d)}{1-\kappa\Delta(\eta(\xi))}. \tag{32}$$

Here, $\bar{A}$ and $\bar{B}$ are constants that are related to the values of $\Phi_n''(\xi_d - \lambda_d)$ and $\Phi_n'''(\xi_d - \lambda_d)$.

Further information on the functional form of $\Phi_n''(\xi)$ cannot be obtained without knowledge of the undamaged mode shape $\Psi_{o,n}(\xi)$ and the mass modification function $\Gamma(\eta(\xi))$. However, a reasonable estimate of the scale of this discontinuity can be found by noting the continuity of the integrand and invoking the Intermediate Value Theorem. This tells us that, for every value of ξ, there must exist a point ξ^*(whose value depends upon ξ) such that $\xi_d - \lambda_d \leqslant \xi^* \leqslant \xi$ and

$$\Phi_n''(\xi) \approx \frac{(\pi/2)^4}{2[1-\kappa\Delta(\eta(\xi))]} \left[\{\Omega_n^2 - 1 - \mu\Omega_n^2 \Gamma(\eta(\xi^*))\}\Psi_{o,n}(\xi^*)\right](\xi - \xi_d + \lambda_d)^2 + \frac{\bar{A} + \bar{B}(\xi - \xi_d + \lambda_d)}{1-\kappa\Delta(\eta(\xi))}. \tag{33}$$

Recalling that we generically expect $\Omega_n^2 \approx 1$ and $\mathcal{O}(\Omega_n^2 - 1) = \mathcal{O}(\varepsilon^{m+2\ell})$, we estimate that the overall size of the first term in the above expression is $\mathcal{O}(\varepsilon^{m+2\ell})$. As for the second term in the above approximation, exact

estimates of the sizes of $\bar{A}$ and $\bar{B}$ are again not possible to make based upon the information available, but we can surmise that this second term will not make a significant contribution to $\Phi_n''(\xi)$ unless $\mathcal{O}(\bar{A}) = \mathcal{O}(\varepsilon^{m+2\ell})$ or lower or $\mathcal{O}(\bar{B}) = \mathcal{O}(\varepsilon^{m+\ell})$ or lower. Assuming that the first term of the approximation is in fact the governing one, we conclude that changes in modal curvature are expected to be quite small (indeed, smaller than the damage-induced mass loss) when mass-affected behavior is relevant.

Following procedures similar to those described above, we can arrive at formal approximations for $\Phi_n'''(\xi)$ and $\Phi_n''''(\xi)$, as well as estimates of their magnitudes. The main results are shown below:

$$\Phi_n'''(\xi) \approx \frac{(\pi/2)^4}{1-\kappa\Delta(\eta(\xi))} - \int_{\xi_d-\lambda_d}^{\xi} \left[\Omega_n^2 - 1 - \mu\Omega_n^2\Gamma(\eta(\xi'))\right]\Psi_{o,n}(\xi')\mathrm{d}\xi' + \frac{\bar{B}}{1-\kappa\Delta(\eta(\xi))}, \quad \mathcal{O}(\Phi_n'''(\xi)) = \mathcal{O}(\varepsilon^{m+\ell}).$$

$$\Phi_n''''(\xi) \approx \left(\frac{\pi}{2}\right)^4 \frac{\left[\Omega_n^2 - 1 - \mu\Omega_n^2\Gamma(\eta(\xi))\right]\Psi_{o,n}(\xi)}{1-\kappa\Delta(\eta(\xi))}, \quad \mathcal{O}(\Phi_n''''(\xi)) = \mathcal{O}(\varepsilon^{m}). \tag{34}$$

As was true of the stiffness-dominated case, we see that higher order derivative discontinuities are anticipated to have larger magnitudes as the order of the derivative increases. None of these terms, however, are expected to be large in any absolute sense, especially since our experience suggests that mass-affected behavior is associated only with very low levels of damage for which mass loss effects should be already rather small. These observations, therefore, compel us to state the caveat that higher order mode shape derivative discontinuities are not guaranteed to provide robust indicators of damage for beam-like structures under all damage scenarios; certain relations must hold among the stiffness loss, mass loss, and damage length scales before robust performance can be obtained.

Once again, we check the quality of this approximate analysis by performing a comparison of approximate and "exact" numerical results. We consider the same simply supported beam problem discussed in Section 4.2.1, but here we choose $\delta = 0.002$ which leads to $\mu = 0.002$ and $\kappa = 8.0 \times 10^{-9}$. This is a clear example of mass-affected behavior, since $\kappa/\lambda_d^2 = 3.2 \times 10^{-6} \ll \mu = 0.002$. In Fig. 24, we show the approximate and numerical results for the fourth derivative discontinuity function; we see a very good level of agreement between the two results. These results, while obviously not a firm proof, do give us confidence that we have captured the underlying discontinuity behavior appropriately with our approximation.

4.2.3. Case 3: inside the damage zone—balanced behavior

The case of balanced behavior presents no new complications as far as obtaining formal approximations of modal derivative discontinuities is concerned. As discussed in Section 3.2.2, the appropriate approximation of the governing equation for modal discontinuities in this case is

$$\frac{\mathrm{d}^2}{\mathrm{d}\xi^2}\left[\{1-\kappa\Delta(\eta(\xi))\}\frac{\mathrm{d}^2\Phi_n(\xi)}{\mathrm{d}\xi^2}\right] \approx \frac{\mathrm{d}^2}{\mathrm{d}\xi^2}\left[\kappa\Delta(\eta(\xi))\frac{\mathrm{d}^2\Psi_{o,n}(\xi)}{\mathrm{d}\xi^2}\right] + \left(\frac{\pi}{2}\right)^4[\Omega_n^2 - 1 - \mu\Omega_n^2\Gamma(\eta(\xi))]\Psi_{o,n}(\xi). \tag{35}$$

The right-hand side of this equation is the sum of the right-hand sides of Eqs. (25) and (31). Linearity of the integration process allows us to conclude that the formal approximations for $\Phi_n''(\xi)$, $\Phi_n'''(\xi)$ and $\Phi_n''''(\xi)$ are simply the sum of the formal approximations derived for the previous two cases; the approximation for $\Phi_n'(\xi)$ is just the sum of the right-hand sides of Eqs. (26) and (32), and similarly for $\Phi_n'''(\xi)$ and $\Phi_n''''(\xi)$.

We check these results by again considering the Mode 1 simply supported beam vibration problem with mid-section cracks from the previous two subsections; in this situation, the damage parameter values are chosen to be $\mu = 0.05$ and $\kappa = 1.25 \times 10^{-4}$, leading to $\kappa/\lambda_d^2 = 0.05 = \mu$. In Fig. 25, we observe the comparison of the exact and analytical results for this case for the fourth derivative discontinuity function in the damage zone; note that the approximate result is the sum of the results shown in Eqs. (30) and (34). Once again, a high level of agreement between the two results is observed. It is interesting to note that, if we decompose the analytical approximation, the stiffness-dominated term from Eq. (30) gives the largest contribution to $\Phi_1''''(\xi)$ in this case. However, the mass-affected term from Eq. (34) is necessary in order to obtain a more exact agreement. Hence, both terms are truly required in order to have a good approximation for balanced behavior.

A condition on the magnitudes of the various damage terms that leads to balanced behavior can be derived by recalling that balanced behavior requires that the two terms on the right-hand side of Eq. (35) be of the

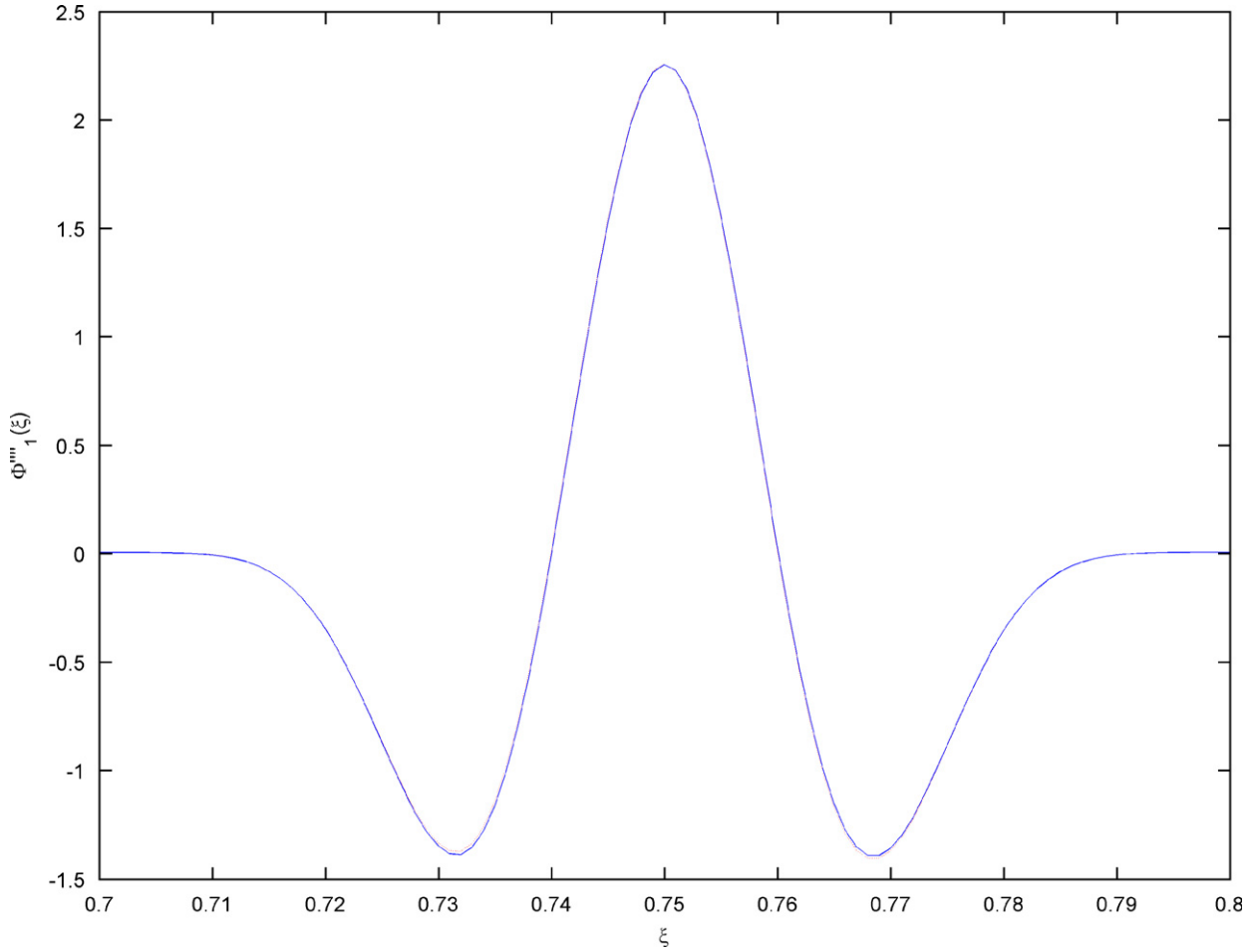

Fig. 25. Comparison of analytical approximations and numerical results for $\Phi''''_1(\xi)$ in the simply supported beam problem with balanced behavior. —— numerical result, · · · analytical approximation.

same order. From our previous analyses, this implies that

$$\mathcal{O}(\varepsilon^{k-2\ell}) = \mathcal{O}(\varepsilon^{m}) \Rightarrow k - 2\ell = m. \tag{36}$$

From this, it can be clearly seen that balanced behavior represents a "boundary" between the stiffness-dominated and mass-affected behaviors. From our order estimates for $T_3(\xi)$ and $T_4(\xi)$, we know that know that $k - 2\ell < m$ defines stiffness-dominated behavior; likewise, mass-affected behavior arises whenever $k - 2\ell > m$. We note that it is possible to have stiffness-dominated behavior without having the mass loss and stiffness loss coefficients be of the same order. For example, a situation like $m = k - \ell$ would lead to "larger" mass loss effects as compared to stiffness loss effects but would still be consistent with overall dominance of the stiffness terms. Examples of this would include the case of mid-section cracks of moderate or relatively large extent; the loss of moment of inertia is still proportional to the cube of the loss of section, while the loss of mass is proportional to section loss, but the magnitude difference between $T_3(\xi)$ and $T_4(\xi)$ decreases as the loss of section increases. This reinforces the suggestion that stiffness-dominated behavior is much more common than the other behaviors observed in this study.

4.3. Special considerations

There are a number of the assumptions made in Section 4 that require special consideration. For example, it was assumed in Section 4.1 that the nondimensional damage radius λ_d scaled as $\bar{\lambda}_d \varepsilon^{\ell}$ with $\ell > 0$. This permitted

us to make conclusions about the relative sizes of various terms in our formal analysis without having to consider too many special situations. However, we acknowledged that $\ell \leqslant 0$ is a physically possible situation expected to occur whenever the damage zone has significant spatial extent or when the wavelength of the mode under consideration becomes sufficiently small. To understand the ramifications of these physical cases, we return to Eq. (36) and the discussion of the roles of k, ℓ, and m in determining the behavior of $\Phi_n(\xi)$ in the damage zone. From these, we observe that $\ell = 0$ (i.e., having the damage radius be comparable in length to the quarter wavelength) turns the balanced behavior condition into $k = m$, and so we generically expect stiffness-dominated behavior whenever the stiffness loss scale exceeds the mass loss scale significantly and mass-affected behavior whenever the mass loss is more significant than stiffness loss. We also anticipate that none of the higher order derivative discontinuities would be large in an absolute sense, as the size of κ or μ (or both) determines the overall magnitude of the discontinuities. One can also surmise that the possible presence of large magnitude values for $\Delta'(\eta)$ or $\Delta''(\eta)$ takes on added importance, as these would make stiffness-dominated behavior more likely to occur (the governing condition becomes $k-d<m$) and would provide a mechanism to generate large discontinuities in $\Phi_n'''(\xi)$ and $\Phi_n'''(\xi)$. As for the case $\ell<0$, we see that this physical situation tilts the expected behavior of the discontinuities more towards mass-affected behavior, since stiffness-dominated or balanced behaviors can now only occur if the stiffness loss effects greatly exceed the mass loss effects. Once again, overall sizes of the discontinuity derivatives would be anticipated as small in this case. Thus, we conclude that having $\ell \leqslant 0$ leads to physical situations that render the higher order modal

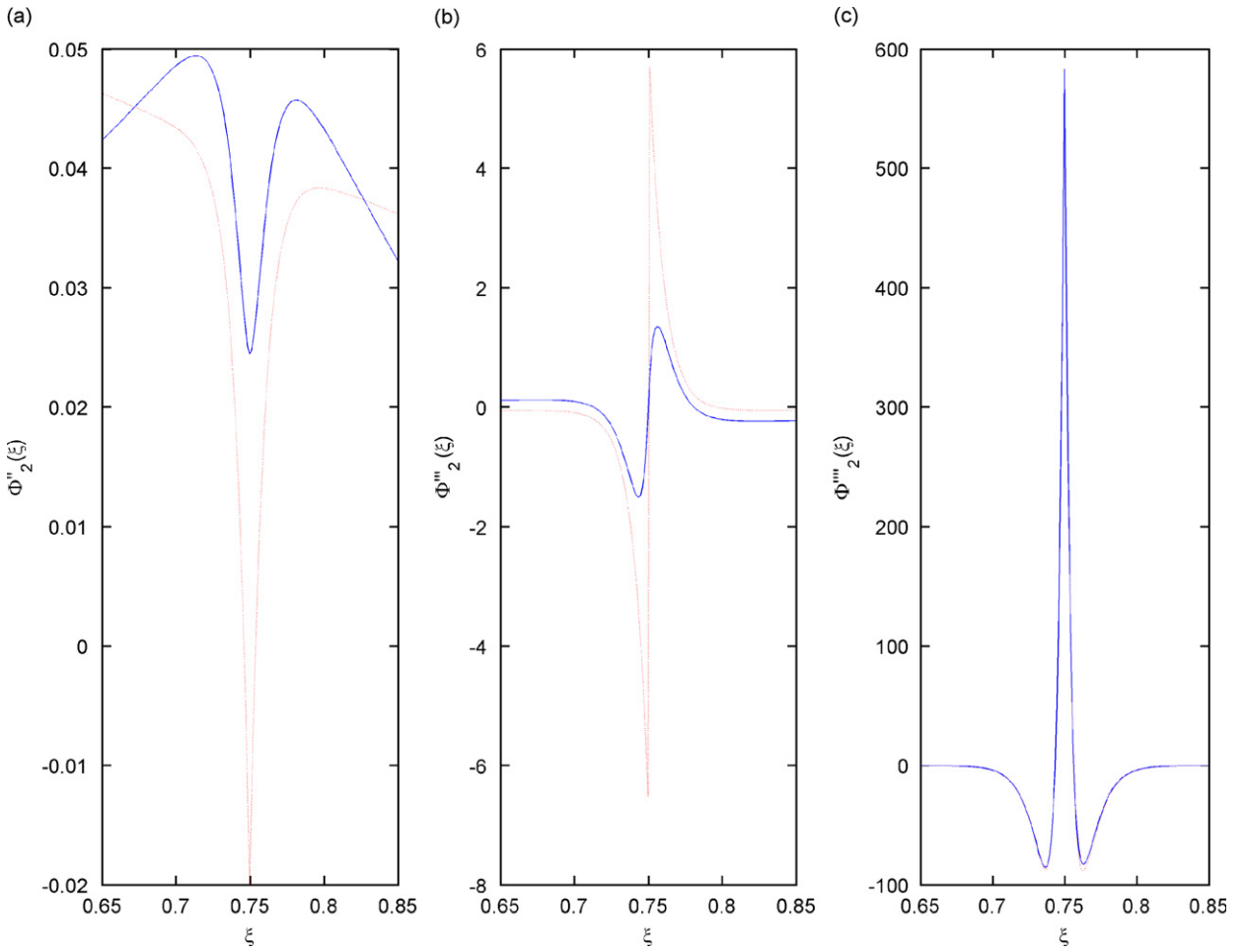

Fig. 26. Comparison of analytical approximations and numerical results for the continuous beam problem using the Christides–Barr damage model. —— numerical result, · · · analytical approximation. (a) $\Phi_1''(\xi)$, (b) $\Phi'''_1(\xi)$, (c) $\Phi''''_1(\xi)$.

derivative discontinuities less effective in indicating the presence of damage, implying that higher modes are not a good choice for use in damage detection and that global damage cases are best detected using other techniques.

The assumption that $\Delta(\eta)$ is $\mathscr{C}^2$-continuous has a more dramatic impact upon the analysis. In fact, many of the conclusions drawn will not hold if the stiffness modification function does not have this level of continuity. For instance, if we permit $\Delta(\eta) = 1 - |\eta|$ to be a valid model of the stiffness loss, $\Delta''(\eta) = -\delta(\eta)$ and the approximation discussed in Section A.1 of the Appendix A for $\Delta''(\eta)$ no longer applies. Analysis of such situations requires the approaches utilized in Ref. [22] or Ref. [23] and will not be pursued in this work. The consequences of violating this assumption can be seen in Fig. 26, where we show a comparison of the analytical approximates and numerical results for the continuous beam problem employing the Christides–Barr damage model. The presence of the $|\eta|$ term in Eq. (19) leads to a discontinuity for $\Delta'(\eta)$ at $\eta = 0$. We considered Mode 2 vibrations and chose $\kappa = 0.03$, $\mu = 0.01010$, $\xi_d = 0.75$, and $\varepsilon = 1.0 \times 10^{-5}$ which led to $\lambda_d = 0.07783$. As seen in the figure, the approximate results do a much poorer job of mimicking the numerical results, particularly for $\Phi'''_n(\xi)$, which is expected to be proportional to $\Delta'(\eta)$. We attribute this to a smoothing of the discontinuities that result from trying to bridge the discontinuous derivative term in a continuous fashion. It should be noted that the assumption of $\mathscr{C}^2$-continuity for $\Delta(\eta)$, while clearly important to this work, is ultimately a modeling choice that allows us to predict behavior of our chosen damage indicator. It is not required that damage present in a real physical system should obey this property; indeed, no such requirements were considered during experimental validation of this damage indicator [31]. Thus, the role that this assumption plays in the analysis needs further consideration.

5. Conclusions

This work has examined the effect that damage has upon second, third, and fourth order derivatives of the mode shapes of structures having primarily beam-like vibration. Via numerical investigations, the sensitivity of various damage related parameters in inducing changes in these higher order modal derivatives was determined, leading to a more complete understanding of what factors make the most contribution to significant changes in these derivatives. We were also able to identify three distinct types of response for the damage-induced higher order derivative discontinuities as three key parameters (the mass loss, stiffness loss, and damage radius scales) were varied. From this, we obtained formal approximations for the expected forms of the higher order derivative discontinuities based upon the underlying behavior predicted by a simple relation among these three parameters. These approximations were checked with numerical simulations, and an excellent level of agreement was observed under appropriate conditions. Finally, we examined the potential of these higher order derivative changes for indicating the presence and location of damage in a global setting.

Summarizing the previous results, we conclude that all of these higher order derivatives are expected to show the effects of damage most prominently inside of the damage zone, making them good indicators of damage location. In contrast, damage was shown to produce global changes in the mode shapes, rendering them less effective at locating damage. All of the higher order modal derivative discontinuities were sensitive to damage level, axial variations in the damage, and the underlying mode shape. More specifically, for the most common type of damage scenario (i.e., stiffness-dominated behavior), all higher order derivative changes were sensitive to maximum stiffness loss and the curvature of the undamaged mode shape. Also, the third and fourth derivative discontinuities showed strong sensitivity to the relative axial size of the damage zone as compared to the modal wavelength, with larger changes being exhibited for smaller relative sizes. Finally, changes in the nth order modal derivative showed a correlation with the $(n-2)$th spatial derivative of the axial variations in damage, leading to the possibility that abrupt changes in damage profile along the beam could manifest themselves as large changes in the third and fourth derivatives. Investigations into the role of mass loss led to the discovery of three distinct types of higher order derivative change, namely the stiffness-dominated, mass-affected, and balanced behaviors. Under the assumption of stiffness-dominated behavior, it was shown that the choice of mass model has very little impact upon modal discontinuities, being relevant only for the higher frequency vibration modes and, even then, diminishing in importance as the modal derivative order increases. When mass-affected behavior or balanced behavior was assumed, the choice of mass model had a much more prominent effect upon the higher order derivative discontinuities.

With the better understanding of the possible types of discontinuity behavior, it was possible to make some approximations to the governing equations and thus obtain formal estimates of the expected changes in the higher order derivative discontinuities for various damage scenarios. The simple relation among stiffness loss, mass loss, and damage radius shown in Eq. (36) allowed us to predict which terms in Eq. (16) (the governing equation for the modal discontinuities) would make the strongest overall contributions, thus permitting us to ignore certain terms and thus obtain simpler equations that could be "solved" for the higher order derivative discontinuities. The accuracy of these predicted changes in the damage zone was demonstrated to be quite good so long as certain continuity assumptions held.

As a related issue, it is our opinion that lower frequency modes are the best choices to analyze for damage-induced modal changes, as higher modes demonstrated less sensitivity to damage radius, more sensitivity to the details of the mass loss, and overall lower levels of change, making damage much harder to detect as the mode number increases. This is, of course, advantageous from an operational point of view, as higher order modes are typically more difficult to detect accurately in the field.

It is worth mentioning that this work merely explores that potential that the various higher order modal derivative changes have in indicating damage. An equally important task is the creation of robust and efficient analysis algorithms that can process experimental data regarding a chosen damage feature and produce a clear, statistically significant indication of damage. The use of fourth order modal derivative discontinuities as a damage feature has a fundamental concern that modal fourth derivatives cannot be obtained from direct physical measurements but instead must be calculated numerically, introducing possible errors. The creation of such algorithms using the fourth order modal derivative discontinuity is on-going [31] and shows promise as a viable global damage detection technique. What this work has shown is that all higher order modal derivative discontinuities display the strong localization and sensitivity properties one desires in a good damage indicator under the assumption of beam-like vibrations. Coupled with a better understanding of the expected modal derivative changes, one can anticipate a variety of improved methods for identifying damage via global vibration measurements resulting from this work.

Appendix A. Order estimates

A.1. Order estimates for derivatives of the stiffness modification function

Since $\Delta(\eta)$ is assumed to be $\mathscr{C}^2$-continuous over $|\eta| \leqslant 1$, we can obtain estimates of $\Delta'(\eta)$ and $\Delta''(\eta)$ at certain points by recalling the assumptions that $\Delta(\eta = 0) = 1$ and that Δ and its derivatives are essentially zero for $|\eta| \geqslant 1$. When we consider the properties $\Delta(\eta = 0) = 1$ and $\Delta(\eta = -1) \approx 0$ and apply the Intermediate Value Theorem, we conclude that there is a point $\eta = \eta_l$ in the damage zone such that

$$\Delta'(\eta = \eta_l) \approx \frac{0 - 1}{-1 - 0} = 1. \tag{A.1}$$

Similarly, considering $\Delta(\eta = 0) = 1$ and $\Delta(\eta = 1) \approx 0$ leads to the result

$$\Delta'(\eta = \eta_r) \approx \frac{0 - 1}{1 - 0} = -1 \tag{A.2}$$

at some point $\eta = \eta_r$ in the damage zone. Both of these quantities are $\mathscr{O}(\varepsilon^0)$ in magnitude. Hence, continuity of $\Delta'(\eta)$ tells us that there are at least two regions in which $\Delta'(\eta)$ takes on $\mathscr{O}(\varepsilon^0)$ values.

As for $\Delta''(\eta)$, if we apply the Intermediate Value Theorem to the previous two slope estimates, we conclude that there is a point $\eta = \eta_c$ in the damage zone such that

$$\Delta''(\eta = \eta_c) \approx \frac{1 - (-1)}{\eta_l - \eta_r} = \frac{2}{\eta_l - \eta_r}. \tag{A.3}$$

Noting that $\eta_r - \eta_l < 2$, we see that $|\Delta''(\eta = \eta_c)|$ is bounded below by the value 1, which in turn implies that $\Delta''(\eta = \eta_c)$ is at least $\mathscr{O}(\varepsilon^0)$ in magnitude. The assumed $\mathscr{C}^2$-continuity then permits us to conclude that a finite-sized portion of the damage zone must have $\mathscr{O}(\varepsilon^0)$ magnitudes for $\Delta''(\eta)$. From these arguments, we see that

both derivatives of the stiffness modification function will attain finite values in the damage zone, although clearly small magnitudes of these derivatives can also exist within this region.

A.2. Order estimate for the frequency ratio

Turning our attention to the frequency ratio Ω_n, we recall that the frequencies of any mode of the system can be evaluated by computing the generalized (modal) stiffness and generalized (modal) mass corresponding to that mode. More specifically, we have the following formulas:

$$\omega_n^2 = \frac{K_n}{M_n}, \quad K_n = \int_0^L EI(x)\,Y_n''(x)^2\mathrm{d}x, \quad M_n = \int_0^L \rho A(x)\,Y_n(x)^2\mathrm{d}x. \tag{A.4}$$

Under our assumptions regarding the flexural rigidity and linear mass density of the damaged system, these expressions can be rewritten in nondimensional form to give

$$\omega_n^2 = \frac{EI_o}{\rho A_o L_{o,n}^4}\int_0^{\Lambda_n}[1-\kappa\Delta(\eta(\xi))]\Psi_n''(\xi)^2\mathrm{d}\xi \Big/ \int_0^{\Lambda_n}[1-\mu\Gamma(\eta(\xi))]\Psi_n(\xi)^2\mathrm{d}\xi. \tag{A.5}$$

If the system is undamaged, the above equation can be simplified:

$$\omega_{o,n}^2 = \frac{EI_o}{\rho A_o L_{o,n}^4}\int_0^{\Lambda_n}\Psi_{o,n}''(\xi)^2\mathrm{d}\xi \Big/ \int_0^{\Lambda_n}\Psi_{o,n}(\xi)^2\mathrm{d}\xi. \tag{A.6}$$

To obtain an approximation for Ω_n^2, we replace $\Psi_n(\xi)$ and $\Psi_n''(\xi)$ with $\Psi_{o,n}(\xi)$ and $\Psi_{o,n}''(\xi)$, respectively, in Eq. (A.5). (The validity of this step will be discussed later.) After performing some algebraic manipulations and using Eq. (A.6), we arrive at the following:

$$\omega_n^2 \approx \omega_{o,n}^2\frac{1-\kappa\psi_\Delta}{1-\mu\psi_\Gamma}, \quad \psi_\Delta = \frac{\int_{\xi_d-\lambda_d}^{\xi_d+\lambda_d}\Delta(\eta(\xi))\Psi_{o,n}''(\xi)^2\mathrm{d}\xi}{\int_0^{\Lambda_n}\Psi_{o,n}''(\xi)^2\mathrm{d}\xi}, \quad \psi_\Gamma = \frac{\int_{\xi_d-\lambda_d}^{\xi_d+\lambda_d}\Gamma(\eta(\xi))\Psi_{o,n}(\xi)^2\mathrm{d}\xi}{\int_0^{\Lambda_n}\Psi_{o,n}(\xi)^2\mathrm{d}\xi} \tag{A.7}$$

Since all of the integrals in ψ_Δ and ψ_Γ involve continuous functions, there must exist four points ξ_1, ξ_2, ξ_3, and ξ_4 such that

$$\psi_\Delta = \frac{2\lambda_d\Delta(\eta(\xi_1))\Psi_{o,n}''(\xi_1)^2}{\Lambda_n\Psi_{o,n}''(\xi_2)^2} \equiv \lambda_d\psi_\Delta^*, \quad \psi_\Gamma = \frac{2\lambda_d\Gamma(\eta(\xi_3))\Psi_{o,n}(\xi_3)^2}{\Lambda_n\Psi_{o,n}(\xi_4)^2} \equiv \lambda_d\psi_\Gamma^*. \tag{A.8}$$

In Eq. (A.8), we note that ψ_Δ^* and ψ_Γ^* are generically of order $\mathcal{O}(\varepsilon^0)$ due to the assumed behaviors of $\Psi_{o,n}(\xi)$, $\Psi_{o,n}''(\xi)$, $\Gamma(\eta(\xi))$, and $\Delta(\eta(\xi))$. Using these results in Eq. (A.7) then leads to

$$\omega_n^2 \approx \omega_{o,n}^2\frac{1-\kappa\lambda_d\psi_\Delta^*}{1-\mu\lambda_d\psi_\Gamma^*}, \text{ or } \Omega_n^2 \approx \frac{1-\kappa\lambda_d\psi_\Delta^*}{1-\mu\lambda_d\psi_\Gamma^*}. \tag{A.9}$$

The above analysis produces an estimate that Ω_n^2 is approximately equal to one, assuming small values for κ, μ, and λ_d. As for Ω_n^2-1, simple algebra gives the following approximation:

$$\Omega_n^2 - 1 \approx \frac{\mu\lambda_d\psi_\Gamma^* - \kappa\lambda_d\psi_\Delta^*}{1-\mu\lambda_d\psi_\Gamma^*}. \tag{A.10}$$

Assuming that κ and μ are of the same order, this expression must be $\mathcal{O}(\varepsilon^{m+\ell})$, since the denominator is close to one in value. Note that the quality of these two approximations hinges upon the accuracy of replacing $\Psi_n(\xi)$ and $\Psi_n''(\xi)$ with $\Psi_{o,n}(\xi)$ and $\Psi_{o,n}''(\xi)$ in Eq. (A.5). The main source of error in this step comes from the fact that $\Psi_n''(\xi)$ is not necessarily close to $\Psi_{o,n}''(\xi)$ in the damage zone. However, the effects of this error are limited, since the damage zone size is still $\mathcal{O}(\varepsilon^\ell)$.

References

[1] S.W. Doebling, C.R. Farrar, M.B. Prime, D.W. Shevitz, Damage identification and health monitoring of structural and mechanical systems from changes in their vibration characteristics: a literature review, Report LA-13070-MS, Los Alamos National Laboratory, Los Alamos, NM, 1996.

[2] H. Sohn, C.R. Farrar, F.M. Hemez, D.D. Shunk, D.W. Stinemates, B.R. Nadler, A review of structural health monitoring literature: 1996–2001, Report LA-13976-MS, Los Alamos National Laboratory, Los Alamos, NM, 2003.

[3] M.M. Abdel Wahab, G. De Roeck, Damage detection in bridges using modal curvatures: application to a real damage scenario, *Journal of Sound and Vibration* 226 (1999) 217–235.

[4] M.I. Friswell, J.E.T. Penney, Is damage location using vibration measurements practical? *EUROMECH 365 International Workshop: DAMAS 97, Structural Damage Assessment using Advanced Signal Processing Procedures,* Sheffield, UK, June/July 1997, pp. 351–362.

[5] M. Biswas, A.K. Pandey, S. Bluni, Modified chain-code computer vision techniques for interrogation of vibration signatures for structural fault detection, *Journal of Sound and Vibration* 175 (1994) 89–104.

[6] P. Cawley, R.D. Adams, The location of defects in structures from measurements of natural frequencies, *Journal of Strain Analysis* 4 (1979) 49–57.

[7] W.M. West, Illustration of the use of modal assurance criterion to detect structural changes in an orbiter test specimen, *Proceedings of the Fourth International Modal Analysis Conference*, February 3–6 1986, Los Angeles, CA, pp. 1–6.

[8] M.M.F. Yuen, A numerical study of the eigenparameters of a damaged cantilever, *Journal of Sound and Vibration* 103 (1985) 301–310.

[9] A.K. Pandey, M. Biswas, M.M. Samman, Damage detection from changes in curvature mode shapes, *Journal of Sound and Vibration* 145 (1991) 321–332.

[10] N. Stubbs, J.-T. Kim, K. Topole, An efficient and robust algorithm for damage localization in offshore platforms, *Proceedings of the ASCE Tenth Structures Congress*, April 13–15, 1992, San Antonio, TX, pp. 543–546.

[11] S.S. Law, P. Waldron, C. Taylor, Damage detection of a reinforced concrete bridge deck using the frequency response function, *Proceedings of the 10th International Modal Analysis Conference*, February 3–7 1992, San Diego, CA, pp. 772–778.

[12] F. Huang, S. Gu, Application of higher order cumulants to structure fault diagnosis, *Proceedings of the 11th International Modal Analysis Conference*, February 1–4 1993, Kissimmee, FL, pp. 1237–1240.

[13] E. Safak, New directions in seismic monitoring of multi-story buildings, in: F.-K. Chang (Ed.), *Structural Health Monitoring, Current Status and Perspectives*, Technomic Publishing, Lancaster, PA, 1997, pp. 418–430.

[14] K.T. Feroz, S.O. Oyadiji, Damage assessment of slotted bars using auto-correlation technique. *Structural Damage Assessment Using Advanced Signal Processing Procedures*, *Proceedings of DAMAS '97*, Sheffield, UK, June/July 1997, pp. 337–348.

[15] P.J. Jacob, M.J. Desforges, A.D. Ball, Analysis of suitable wavelet coefficients for identification of the simulated failure of composite materials, *Structural Damage Assessment Using Advanced Signal Processing Procedures*, *Proceedings of DAMAS '97*, Sheffield, UK, June/July 1997, pp. 31–40.

[16] C. Modena, D. Sonda, D. Zonta, Damage localization in reinforced concrete structures by using damping measurements, *Damage Assessment of Structures*, *Proceedings of the International Conference on Damage Assessment of Structures (DAMAS '99)*, Dublin, Ireland, June 1999, pp. 132–141.

[17] H.T. Vincent, S.-L.J. Hu, Z. Hou, Damage detection using empirical mode decomposition method and a comparison with wavelet analysis, in: F.-K. Chang (Ed.), *Structural Health Monitoring 2000*, Technomic Publishing, Lancaster, PA, 1999, pp. 891–900.

[18] H. Sohn, C.R. Farrar, Statistical process control and projection techniques for damage detection, *European COST F3 Conference on System Identification and Structural Health Monitoring*, Madrid, Spain, June 2000, pp. 105–114.

[19] M.A.-B. Abdo, M. Hori, A numerical study of structural damage detection using changes in the rotation of mode shapes, *Journal of Sound and Vibration* 251 (2002) 227–239.

[20] J.F. Gauthier, The Higher Order Derivative Discontinuity Method for Nondestructive Evaluation and Rating of Bridges, PhD Thesis, Purdue University, West Lafayette, IN, 2005.

[21] L. Meirovitch, *Analytical Methods in Vibrations*, Macmillan, New York, 1967.

[22] A. Yavari, S. Sarkani, E.T. Moyer Jr., On applications of generalized functions to beam bending problems, *International Journal of Solids and Structures* 37 (2000) 5675–5705.

[23] B. Biondi, S. Caddemi, Closed form solutions of Euler–Bernoulli beams with singularities, *International Journal of Solids and Structures* 42 (2005) 3027–3044.

[24] S. Christides, A.D.S. Barr, One-dimensional theory of cracked Bernoulli–Euler beams, *International Journal of Mechanical Sciences* 26 (1984) 639–648.

[25] M.-H.H. Shen, C. Pierre, Natural modes of Bernoulli–Euler beams with symmetric cracks, *Journal of Sound and Vibration* 138 (1990) 115–134.

[26] T.G. Chondros, The continuous crack flexibility model for crack identification, *Fatigue and Fracture in Engineering Materials and Structures* 24 (2001) 643–650.

[27] S.H.S. Carneiro, D.J. Inman, Continuous model for the transverse vibration of cracked Timoshenko beams, *Journal of Vibration and Acoustics* 124 (2002) 310–320.

[28] M.M. Abdel Wahab, G. De Roeck, B. Peeters, Parameterization of damage in reinforced concrete structures using model updating, *Journal of Sound and Vibration* 228 (1999) 717–730.

[29] J.K. Sinha, M.I. Friswell, S. Edwards, Simplified models for the location of cracks in beam structures using measured vibration data, *Journal of Sound and Vibration* 251 (2002) 13–38.
[30] R.D. Blevins, *Formulas for Natural Frequency and Mode Shape*, Krieger, Malabar, FL, 2001.
[31] J.F. Gauthier, T.M. Whalen, T.M., J. Liu, Experimental validation of the higher order derivative discontinuity method for damage identification, *Journal of Structural Control and Health Monitoring* (2007), in press, doi:10.1002/stc.210.